

Colloquium: Spontaneous magnon decays

M. E. Zhitomirsky

Service de Physique Statistique, Magnétisme et Supraconductivité, UMR-E9001, CEA-INAC/UJF, 17 rue des Martyrs, 38054 Grenoble cedex 9, France

A. L. Chernyshev

Department of Physics, University of California, Irvine, California 92697, USA

(published 23 January 2013)

A theoretical overview of the phenomenon of spontaneous magnon decays in quantum antiferromagnets is presented. The intrinsic zero-temperature damping of magnons in quantum spin systems is a fascinating many-body effect, which has recently attracted significant attention in view of its possible observation in neutron-scattering experiments. An introduction to the theory of magnon interactions and a discussion of necessary symmetry and kinematic conditions for spontaneous decays are provided. Various parallels with the decays of anharmonic phonons and excitations in superfluid ^4He are extensively used. Three principal cases of spontaneous magnon decays are considered: field-induced decays in Heisenberg antiferromagnets, zero-field decays in spiral antiferromagnets, and triplon decays in quantum-disordered magnets. Analytical results are compared with available numerical data and prospective materials for experimental observation of the decay-related effects are briefly discussed.

DOI: [10.1103/RevModPhys.85.219](https://doi.org/10.1103/RevModPhys.85.219)

PACS numbers: 75.30.Ds, 75.10.Jm, 75.50.Ee

CONTENTS

I. Introduction	219
II. Magnon-magnon Interactions	220
A. Four-magnon interactions	221
B. Three-magnon interactions	221
C. Magnon self-energies	222
D. Three-boson interactions in spin liquids	222
III. Kinematics of Two-magnon Decays	223
A. Decay threshold boundary	223
B. Decay of acoustic excitations	223
1. Single acoustic branch	224
2. Several acoustic branches	224
C. Decay singularities	224
IV. Field-induced Decays	225
A. General discussion	225
B. Square-lattice antiferromagnet	226
1. Model and formalism	227
2. Decay region	227
C. Spectral function and self-consistent Born approximation	228
D. Decay singularities and SCBA	229
E. Decays in three dimensions	231
V. Zero-field Decays	231
A. General discussion	232
B. Triangular-lattice antiferromagnet	232
VI. Damping of Low-energy Magnons	234
VII. Magnon Decay in Quantum Spin Liquids	236
A. Bond-operator formalism	236
B. Termination point of the magnon branch	237
C. Decay of longitudinal magnons	239
VIII. Summary and Outlook	240
Acknowledgments	241
References	241

I. INTRODUCTION

According to conventional wisdom a quasiparticle is presumed well defined until proven not to be. The textbook picture of magnons as long-lived excitations weakly interacting with each other works very well for many magnetic materials. Nevertheless, in a number of recently studied spin systems magnons neither interact weakly nor remain well defined even at zero temperature. This is due to the so-called spontaneous decay, a spectacular quantum-mechanical many-body effect, which is the topic of the current Colloquium.

Magnetic excitations have been the subject of intensive theoretical and experimental studies since the first half of the last century. Historically, the concept of spin waves was introduced by Bloch (1930) and, independently, by Slater (1930) for the wavelike propagation of spin flips in ordered ferromagnets; see also Hoddeson, Baym, and Eckert (1987). Already in his earliest work Bloch (1930) described spin waves as weakly interacting excitations obeying Bose statistics. Subsequently, Holstein and Primakoff (1940) introduced second quantization of spin waves in terms of bosonic operators, the approach widely used to this day. The first use of the word “magnon,” which concisely unifies the notions of an elementary quasiparticle and a magnetic quantum, can be traced back to Pomeranchuk (1941), who ascribed this term to Lev Landau; see Walker and Slack (1970). Although the terms “spin waves” and “magnons” are sometimes used to distinguish between long- and short-wavelength excitations, respectively, in the following we use both names interchangeably.

In addition, the fundamental contribution to the theory of spin waves in magnetic insulators was made by Anderson (1952), Kubo (1952), and Dyson (1956a, 1956b). These and subsequent studies developed a comprehensive picture of spin

waves in conventional quantum ferromagnets and antiferromagnets, which can be found in various reviews and books; see [Van Kranendonk and Van Vleck \(1958\)](#), [Akhiezer, Bar'yakhtar, and Peletminskii \(1968\)](#), [Mattis \(1981\)](#), [White \(1983\)](#), [Borovik-Romanov and Sinha \(1988\)](#), [Manousakis \(1991\)](#), and [Majlis \(2007\)](#). Invented in the 1950s, inelastic neutron-scattering spectroscopy ([Brockhouse, 1995](#)) has quickly become a major experimental method of investigating spin waves and other magnetic excitations in solids. With a variety of specialized techniques currently used at numerous neutron facilities around the world, it remains the most powerful and versatile research tool for studies of magnetic spectra. Other microscopic techniques to investigate excitations in magnetic materials are electron spin resonance ([Gurevich and Melkov, 1996](#)) and light scattering methods, such as resonant inelastic x-ray scattering ([Beaurepaire, 2006](#)).

Usually, the magnon-magnon interactions play a minor role at low temperatures. For example, as $T \rightarrow 0$ deviation of the spontaneous magnetization of a ferromagnet from its saturated value follows Bloch's law $\Delta M \propto T^{3/2}$, the result obtained by considering magnons as noninteracting bosons. Interactions yield a correction to Bloch's law that scales as T^4 , which is still smaller than the "kinematic" correction proportional to $T^{5/2}$ due to deviation of magnon dispersion from its parabolic form ([Dyson, 1956b](#)). In antiferromagnets, the effects of magnon-magnon interaction survive at zero temperature due to zero-point motion in the ground state. An estimate of their role is given by the magnitude of the quantum correction to the magnon dispersion law obtained in the harmonic, or semiclassical, approximation. Even in low dimension (2D) and even in the "extreme quantum" case of $S = 1/2$, such a correction for the square-lattice Heisenberg antiferromagnet amounts to a mere $\sim 16\%$ rescaling of the harmonic dispersion ([Manousakis, 1991](#)).

Recently, there has been a growing body of theoretical and experimental studies showing that the conventional picture of magnons as weakly interacting quasiparticles is not always correct. The first class of systems exhibiting significant deviations from the conventional semiclassical dynamics is weakly coupled antiferromagnetic chains, for which the spin-wave approximation is not a good starting point. Their high-energy spectra are well described by propagating one-dimensional spinons, the natural basis for excitations in spin- $\frac{1}{2}$ chains ([Schulz, 1996](#); [Coldea et al., 2001](#); [Kohno, Starykh, and Balents, 2007](#)). Since the development of a quantitative theory for the 1D to 3D crossover in weakly coupled chains is still in progress, we shall not discuss this physics here.

The second class is, in a sense, simpler and more puzzling at the same time. It is comprised of quantum magnets with well-ordered ground states whose dynamical properties are yet quite different from the predictions of harmonic spin-wave theory ([Zheng et al., 2006a](#)). In the following, we focus on this second class of unconventional magnetic systems. It includes quantum magnets with noncollinear spin ordering. The key role in their unusual dynamical properties is played by cubic anharmonicities, or three-magnon processes, which originate from the noncollinearity of spins. Three-magnon processes are absent in conventional collinear

antiferromagnets, making their spin-wave excitations intrinsically weakly interacting. The most striking effect of three-magnon interactions is the finite lifetime of spin waves: not only at nonzero temperatures when magnon linewidth is determined by scattering off thermal excitations, but also at $T = 0$ when damping is produced by *spontaneous* magnon decays.

In order to put the phenomenon of spontaneous magnon decays in a broader context, we note that two other subfields of condensed matter physics also deal with decays of bosonic excitations. These are anharmonic crystals ([Kosevich, 2005](#)) and superfluid liquids and gases ([Lifshitz and Pitaevskii, 1980](#); [Pethick and Smith, 2008](#)). Cubic anharmonicities are naturally present in these systems, but their role differs both quantitatively and qualitatively from that in quantum spin systems. In crystals, the anharmonic corrections are generally small due to small mean fluctuations of ions around equilibrium positions, the condition satisfied for the majority of solids below the Debye temperature. In superfluids, the strength of cubic interactions is determined by the condensate fraction and may again become small, as is the case of superfluid ^4He . Quantum magnets are unique in that (i) cubic anharmonicities may be tuned on and off by an external magnetic field or by changing the lattice geometry, and (ii) the existing variety of magnetic compounds provides a diverse choice of magnon dispersion laws $\varepsilon_{\mathbf{k}}$, which play key roles in spontaneous quasiparticle decays. Still, various parallels and analogies between the three branches of condensed matter physics prove to be helpful and will be extensively used in the subsequent discussion.

The rest of the article is organized as follows. Section II contains a general discussion of the origin of cubic as well as quartic anharmonicities in quantum magnets. The energy and momentum conservation conditions for spontaneous decays and the decay-induced singularities in two-dimensional spin systems are analyzed in Sec. III. In Sec. IV we provide a description of spontaneous magnon decays in the square-lattice Heisenberg antiferromagnet in strong external field, while Sec. V deals with another prototypical noncollinear magnet: the triangular-lattice Heisenberg antiferromagnet in zero field. A few general scenarios of the decay of long-wavelength excitations are considered in Sec. VI. Section VII is devoted to the discussion of the role of cubic anharmonicities in gapped quantum spin liquids. Finally, a summary and outlook are presented in Sec. VIII.

II. MAGNON-MAGNON INTERACTIONS

In the classical picture, the interaction between magnons is related to the amplitude of spin precession and can become arbitrarily small as the amplitude decreases. Zero-point motion of spins puts a lower bound on the amplitude and leads to non-negligible interaction effects in quantum magnets. Usually, the consideration of magnon-magnon interactions begins with a discussion of bosonic representations for spin operators. Here we intentionally skip this step, postponing technical details to the subsequent sections. Instead, we discuss the general structure of effective bosonic Hamiltonians defined solely by the symmetry of the magnetic ground state and corresponding excitations.

A. Four-magnon interactions

To draw an analogy between different bosonic systems we begin with the Hamiltonian of a normal Bose gas

$$\hat{\mathcal{H}}_0 = \sum_{\mathbf{k}} \varepsilon_{\mathbf{k}} a_{\mathbf{k}}^\dagger a_{\mathbf{k}} + \frac{1}{4} \sum_{\mathbf{k}_i} V_4^{(0)}(\mathbf{k}_1, \mathbf{k}_2; \mathbf{k}_3, \mathbf{k}_4) a_{\mathbf{k}_1}^\dagger a_{\mathbf{k}_2}^\dagger a_{\mathbf{k}_3} a_{\mathbf{k}_4} + \dots, \quad (1)$$

where $\varepsilon_{\mathbf{k}}$ is the kinetic energy, $V_4^{(0)}(\mathbf{k}_1, \mathbf{k}_2; \mathbf{k}_3, \mathbf{k}_4)$ is the two-particle scattering amplitude, the ellipsis stands for n -particle interactions, and momentum conservation is assumed from now on for various \mathbf{k} summations. The interaction term in Eq. (1) conserves the number of particles, a natural constraint for liquid helium or cold atomic gases. At the same time, an effective bosonic Hamiltonian with exactly the same structure as in Eq. (1) describes the quantum Heisenberg ferromagnet (Holstein and Primakoff, 1940; Oguchi, 1960). Although the number of quasiparticles may not be conserved, in a ferromagnet the conservation is enforced by the invariance of the ground state under an arbitrary rotation about the magnetization direction. Because of this symmetry the ground state and all excitations are characterized by definite values of the z projection of the total spin S^z , from $S_{\text{tot}}^z = NS$ and down. Consequently, the matrix elements of the Hamiltonian vanish for states with different spin projections, resulting in the particlelike form of the interaction term in Eq. (1). In other words, in the Heisenberg ferromagnet every magnon has an intrinsic quantum number $\Delta S^z = -1$, which is conserved in magnon scattering processes.

The quasiparticle-number conservation does not hold for interaction processes in quantum antiferromagnets. As pointed out by Anderson (1984), the symmetry-broken antiferromagnetic ground state corresponds to a superposition of states with different values of the total spin. Hence, elementary excitations cannot be assigned with a definite value of spin: the spin of the spin wave ceases to exist. Because of that, the effective Hamiltonian of a quantum antiferromagnet contains additional interaction terms,

$$\hat{\mathcal{H}}_4 = \frac{1}{3!} \sum_{\mathbf{k}_i} V_4^{(1)}(\mathbf{k}_1, \mathbf{k}_2, \mathbf{k}_3; \mathbf{k}_4) (a_{\mathbf{k}_1}^\dagger a_{\mathbf{k}_2}^\dagger a_{\mathbf{k}_3}^\dagger a_{\mathbf{k}_4} + \text{H.c.}) + \frac{1}{4!} \sum_{\mathbf{k}_i} V_4^{(2)}(\mathbf{k}_1, \mathbf{k}_2, \mathbf{k}_3, \mathbf{k}_4) (a_{\mathbf{k}_1}^\dagger a_{\mathbf{k}_2}^\dagger a_{\mathbf{k}_3}^\dagger a_{\mathbf{k}_4}^\dagger + \text{H.c.}), \quad (2)$$

that do not conserve the number of excitations; see, for example, Harris *et al.* (1971). The first term in Eq. (2) describes decay and recombination processes of one magnon into three and vice versa, whereas the second, so-called source term, corresponds to creation and annihilation of four particles out of (into) an antiferromagnetic vacuum.

B. Three-magnon interactions

Another type of anharmonicity that may appear in an effective bosonic Hamiltonian is the three-particle interaction term. In a generic quantum system with nonconserved number of particles anharmonicities of all orders are present,

beginning with the lowest-order cubic terms, which couple one- and two-particle states. For instance, cubic terms represent the dominant anharmonicity for lattice vibrations (Kosevich, 2005). However, additional symmetry restrictions may forbid such cubic interactions in antiferromagnets.

In the case of a collinear antiferromagnet, the remaining SO(2) rotational symmetry about the Néel vector direction (z axis) prohibits cubic terms. Although the single-magnon state is not an eigenstate of the S_{tot}^z operator, such a state still preserves an odd parity under the π rotation about the z axis. In contrast, the two-magnon states are invariant under this symmetry operation. Consequently, the coupling between one- and two-particle sectors is strictly forbidden in collinear antiferromagnets and cubic terms do not occur in their effective bosonic description. In hindsight, this lack of low-degree anharmonicities explains why the spin-wave theory works quantitatively well even for spin- $\frac{1}{2}$ systems: magnets with collinear spin structures have excitations that are intrinsically weakly interacting.

On the other hand, three-magnon interaction terms must be present if the spin-rotational symmetry is completely broken in the ground state, i.e., when the magnetic structure becomes noncollinear. This is realized, for example, due to spin canting in an applied magnetic field or because of competing interactions in frustrated antiferromagnets. The general form of the three-boson interaction is given by

$$\hat{\mathcal{H}}_3 = \frac{1}{2!} \sum_{\mathbf{k}_i} V_3^{(1)}(\mathbf{k}_1, \mathbf{k}_2; \mathbf{k}_3) (a_{\mathbf{k}_1}^\dagger a_{\mathbf{k}_2}^\dagger a_{\mathbf{k}_3} + \text{H.c.}) + \frac{1}{3!} \sum_{\mathbf{k}_i} V_3^{(2)}(\mathbf{k}_1, \mathbf{k}_2, \mathbf{k}_3) (a_{\mathbf{k}_1}^\dagger a_{\mathbf{k}_2}^\dagger a_{\mathbf{k}_3}^\dagger + \text{H.c.}), \quad (3)$$

where the first term describes the two-particle decay and recombination processes while the second is another source term.

There exists a deep analogy between the noncollinear quantum magnets and superfluid boson systems regarding the presence of cubic interactions in their effective Hamiltonians. The Bose gas in the normal state is invariant under the group of gauge transformations U(1) and is described by the Hamiltonian (1). The macroscopic occupation of the lowest-energy state $\langle a_{\mathbf{k}=0} \rangle \neq 0$ below the superfluid transition leads to breaking of the U(1) symmetry and, at the same time, to the appearance of the cubic terms by virtue of the Bogolyubov substitution

$$a_{\mathbf{k}_1}^\dagger a_{\mathbf{k}_2}^\dagger a_{\mathbf{k}_3} a_{\mathbf{k}_4} \rightarrow a_{\mathbf{k}_1}^\dagger a_{\mathbf{k}_2}^\dagger a_{\mathbf{k}_3} \langle a_0 \rangle + \dots \quad (4)$$

In other words, the vacuum state with the Bose condensate absorbs or emits an extra particle, enabling nonconserving processes between excitations.

An analogous consideration of the noncollinear magnetically ordered state is possible, leading to the same qualitative answer. In fact, it was realized a long time ago by Matsubara and Matsuda (1956) and by Batyev and Braginskii (1984) that there is a one-to-one correspondence between breaking the SO(2) rotational invariance about the field direction for Heisenberg and planar magnets and breaking the U(1) gauge symmetry at the superfluid transition. Noncollinear magnetic structures stabilized by competing exchange interactions in zero field belong to a different class as they spontaneously

break the full SO(3) rotational symmetry without the help of an external field. Still, the absence of any remaining symmetry constraints for their elementary excitations, apart from energy and momentum conservation, permits all possible anharmonic terms including the cubic ones.

It is necessary to mention that cubic anharmonicities due to the long-range dipolar interactions have been discussed already in the early works on the quantum theory of spin waves in ferromagnets (Holstein and Primakoff, 1940; Akhiezer, Bar'yakhtar, and Peletminskii, 1968), where they play an important role in the low-frequency magnetization dynamics (Gurevich and Melkov, 1996; Chernyshev, 2012). However, the effect of cubic terms is completely negligible at higher energies because of the smallness of the dipole-dipole interaction compared to the exchange energy. In contrast, cubic anharmonicities discussed in this work are of exchange origin and have a profound effect on the magnon excitation spectra.

Anharmonic interactions are not restricted to cubic and quartic processes. The usual spin-wave expansion based on the Holstein-Primakoff transformation for spin operators produces an infinite series of interaction terms. Typically, these higher-order terms are small due to the spin-wave expansion parameter $\langle a^\dagger a \rangle / 2S \ll 1$ associated with each order of expansion. We disregard them in the following analysis as they do not alter our results, either qualitatively or quantitatively.

C. Magnon self-energies

Magnon interactions play a dual role. On the one hand, they renormalize magnon energy and, on the other hand, they can lead to magnon decay and result in a finite lifetime. Both effects are treated on equal footing within the standard Green's function approach (Lifshitz and Pitaevskii, 1980; Mahan, 2000). The lowest-order self-energy diagrams produced by three- and four-particle vertices at $T = 0$ are shown in Fig. 1. Analytic expressions for Figs. 1(a) and 1(b) are

$$\begin{aligned}\Sigma_a(\mathbf{k}, \omega) &= \frac{1}{2} \sum_{\mathbf{q}} \frac{|V_3^{(1)}(\mathbf{q}; \mathbf{k})|^2}{\omega - \varepsilon_{\mathbf{q}} - \varepsilon_{\mathbf{k}-\mathbf{q}} + i0}, \\ \Sigma_b(\mathbf{k}, \omega) &= -\frac{1}{2} \sum_{\mathbf{q}} \frac{|V_3^{(2)}(\mathbf{q}, \mathbf{k})|^2}{\omega + \varepsilon_{\mathbf{q}} + \varepsilon_{\mathbf{k}+\mathbf{q}}},\end{aligned}\quad (5)$$

whereas the three-magnon decay process of Fig. 1(c) gives

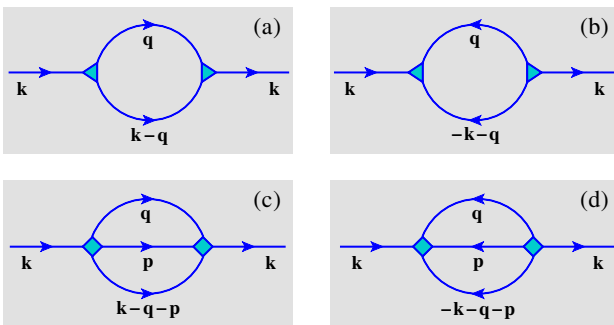


FIG. 1 (color online). Zero-temperature self-energy diagrams due to the (a) and (b) three-magnon, and (c) and (d) four-magnon interactions.

$$\Sigma_c(\mathbf{k}, \omega) = \frac{1}{6} \sum_{\mathbf{q}, \mathbf{p}} \frac{|V_4^{(1)}(\mathbf{q}, \mathbf{p}; \mathbf{k})|^2}{\omega - \varepsilon_{\mathbf{q}} - \varepsilon_{\mathbf{p}} - \varepsilon_{\mathbf{k}-\mathbf{q}-\mathbf{p}} + i0}. \quad (6)$$

We included only independent momenta in the arguments of vertices in Eqs. (5) and (6).

In the lowest order of perturbation theory, the real part of the on-shell self-energy $\Sigma(\mathbf{k}, \omega = \varepsilon_{\mathbf{k}})$ gives a correction to the dispersion $\delta\varepsilon_{\mathbf{k}}$, and the imaginary part yields the decay rate $\Gamma_{\mathbf{k}} = -\text{Im}\Sigma(\mathbf{k}, \varepsilon_{\mathbf{k}})$. The source diagrams in Figs. 1(b) and 1(d) have no imaginary parts, while the magnon damping resulting from the decay diagram in Fig. 1(a) is given by

$$\Gamma_{\mathbf{k}}^{(3)} = \frac{\pi}{2} \sum_{\mathbf{q}} |V_3^{(1)}(\mathbf{q}; \mathbf{k})|^2 \delta(\varepsilon_{\mathbf{k}} - \varepsilon_{\mathbf{q}} - \varepsilon_{\mathbf{k}-\mathbf{q}}). \quad (7)$$

The three-particle decay process in Fig. 1(c) yields a similar expression

$$\Gamma_{\mathbf{k}}^{(4)} = \frac{\pi}{6} \sum_{\mathbf{q}} |V_4^{(1)}(\mathbf{q}, \mathbf{p}; \mathbf{k})|^2 \delta(\varepsilon_{\mathbf{k}} - \varepsilon_{\mathbf{q}} - \varepsilon_{\mathbf{p}} - \varepsilon_{\mathbf{k}-\mathbf{q}-\mathbf{p}}). \quad (8)$$

Existence of the decay amplitudes $V_3^{(1)}$ and $V_4^{(1)}$ is a necessary, but by no means sufficient, condition for spontaneous magnon decays. The decay rate $\Gamma_{\mathbf{k}}$ is nonzero only if the energy conservation is satisfied for at least one decay channel. A general analysis of the kinematic conditions following from the energy conservation for two-particle decays is given in Sec. III.

D. Three-boson interactions in spin liquids

Apart from magnetically ordered antiferromagnets, there is a wide class of quantum-disordered magnets with spin-liquid-like ground states. At zero temperature such magnets remain completely isotropic under spin rotations and their ground-state wave function is a singlet state of the total spin $S_{\text{tot}} = 0$; see Sec. VII for more detailed discussion and references. In spin-dimer systems and in some gapped chain materials, the low-energy excitations are $S = 1$ magnons separated by a finite gap from the singlet ground state. This means that at any given momentum \mathbf{k} there is a triplet of excited states with the same energy $\varepsilon_{\mathbf{k}}$. We use bosonic operators $t_{\mathbf{k}\alpha}^\dagger$ and $t_{\mathbf{k}\alpha}$ with $\alpha = x, y,$ and z to describe creation or annihilation of such quasiparticles, which are also called triplons. Having an intrinsic quantum number, spin polarization α , does not change appreciably the structure of the quartic terms in Eqs. (1) and (2): the SO(3)-invariant anharmonic interactions are constructed by making all possible convolutions for two pairs of polarization indices. An interesting observation is that in this case the spin-rotational symmetry does not forbid the cubic vertices. The total spin is conserved since two spin-1 magnons can form a state with the same total spin $S_{\text{tot}} = 1$. The invariant form of the cubic interaction for triplons is then given by

$$\hat{\mathcal{H}}_3 = \frac{1}{2!} \sum_{\mathbf{k}_i} V_3(\mathbf{k}_1, \mathbf{k}_2; \mathbf{k}_3) \varepsilon^{\alpha\beta\gamma} (t_{\mathbf{k}_1\alpha}^\dagger t_{\mathbf{k}_2\beta}^\dagger t_{\mathbf{k}_3\gamma} + \text{H.c.}), \quad (9)$$

where the conservation of total spin is imposed by the antisymmetric tensor $\varepsilon^{\alpha\beta\gamma}$. In addition, there are certain lattice symmetries affecting the structure of the decay vertex

in Eq. (9), which may still forbid the two-particle decays of triplons. Specific examples of that are discussed in Sec. VII.

III. KINEMATICS OF TWO-MAGNON DECAYS

The aim of this section is to consider kinematic constraints in the two-particle decay process that follow from energy conservation:

$$\varepsilon_{\mathbf{k}} = \varepsilon_{\mathbf{q}} + \varepsilon_{\mathbf{k}-\mathbf{q}}. \quad (10)$$

For a magnon with the momentum \mathbf{k} , the relation (10) is an equation for an unknown \mathbf{q} with \mathbf{k} being an external parameter. Solutions of Eq. (10) form a decay *surface*, the locus of momenta of quasiparticles created in the decay. As a function of the initial momentum \mathbf{k} the decay surface expands or shrinks and may disappear completely. In the latter case, the magnon with momentum \mathbf{k} becomes stable. The region in \mathbf{k} space with stable excitations is separated from the decay *region* where decays are allowed by the decay *threshold boundary*.

For any given \mathbf{k} the two-particle excitations form a continuum of states in a certain energy interval

$$E_2^{\min}(\mathbf{k}) \leq E_2(\mathbf{k}, \mathbf{q}) \equiv \varepsilon_{\mathbf{q}} + \varepsilon_{\mathbf{k}-\mathbf{q}} \leq E_2^{\max}(\mathbf{k}). \quad (11)$$

With the help of this statement it is straightforward to see that nontrivial solutions of Eq. (10) exist only if the single-particle branch and the two-particle continuum overlap. From this perspective it also becomes evident that the decay threshold boundary must be the surface of intersections of the single-particle branch $\varepsilon_{\mathbf{k}}$ with the *bottom* of the continuum $E_2^{\min}(\mathbf{k})$.

Suppose for a moment that spontaneous two-particle decays are completely forbidden, i.e., the one-magnon branch lies below the two-magnon continuum in the whole Brillouin zone,

$$\varepsilon_{\mathbf{k}} \leq \varepsilon_{\mathbf{q}} + \varepsilon_{\mathbf{k}-\mathbf{q}} \quad \text{for } \forall \mathbf{k}, \mathbf{q}, \quad (12)$$

where the equality may be realized only for a trivial solution $\mathbf{q} = \mathbf{0}$, provided that $\varepsilon_0 = 0$. Applying the same relation (12) to $\varepsilon_{\mathbf{k}-\mathbf{q}}$ on the right-hand side gives

$$\varepsilon_{\mathbf{k}} \leq \varepsilon_{\mathbf{q}} + \varepsilon_{\mathbf{p}} + \varepsilon_{\mathbf{k}-\mathbf{q}-\mathbf{p}} \quad \text{for } \forall \mathbf{q}, \mathbf{p}, \quad (13)$$

which means that the one-magnon branch also lies below the three-magnon continuum as well as any n -magnon continua. Thus, if two-particle decays of Eq. (10) are prohibited for any value of \mathbf{k} , the energy and momentum conservation also forbid decays in all n -particle channels with $n \geq 3$ (Harris *et al.*, 1971). This is why it is important to analyze kinematic conditions for two-particle decays as the first step even if the cubic terms are not present.

Aside from finding whether spontaneous decays exist or not, there is another reason for considering kinematics of decays. Investigating two-roton decays in the superfluid ^4He , Pitaevskii (1959) found that the enhanced density of states (DoS) near the bottom of the two-particle continuum may produce strong singularities in the single-particle spectrum at the decay threshold boundary. Additional singularities may also occur inside the decay region due to topological transitions of the decay surface (Chernyshev and Zhitomirsky,

2006). A general analysis of these two effects is given in Sec. III.C.

A. Decay threshold boundary

The bottom of the two-particle continuum can be found by imposing the extremum condition $\nabla_{\mathbf{q}} E_2(\mathbf{k}, \mathbf{q}) = 0$, which is satisfied if the velocities of two magnons are equal,

$$\mathbf{v}_{\mathbf{q}} = \mathbf{v}_{\mathbf{k}-\mathbf{q}}. \quad (14)$$

Using this, the decay threshold boundary is determined by the system of equations (10) and (14). One can distinguish several types of general solutions, or decay channels, for such boundaries (Lifshitz and Pitaevskii, 1980; Chernyshev and Zhitomirsky, 2006):

- (i) The emission of two equivalent magnons with equal momenta $\mathbf{q} = \mathbf{k} - \mathbf{q} = \frac{1}{2}(\mathbf{k} + \mathbf{G})$, where \mathbf{G} is a reciprocal lattice vector. In this case Eq. (14) is satisfied automatically while Eq. (10) is reduced to

$$\varepsilon_{\mathbf{k}} = 2\varepsilon_{(\mathbf{k}+\mathbf{G})/2}. \quad (15)$$

- (ii) The emission of an acoustic magnon with $\mathbf{q} \rightarrow \mathbf{0}$. In this case Eq. (10) is fulfilled while Eq. (14) is equivalent to

$$|\mathbf{v}_{\mathbf{k}}| = |\mathbf{v}_0|. \quad (16)$$

- (iii) The emission of an acoustic magnon with $\mathbf{q} \rightarrow \mathbf{Q}_i$ (for magnets with several acoustic branches):

$$\varepsilon_{\mathbf{k}} = \varepsilon_{\mathbf{k}-\mathbf{Q}_i}. \quad (17)$$

- (iv) The emission of two finite-energy magnons with different energies but the same velocities. No simplification occurs in this case.

The resultant decay region is given by the union of all subregions enclosed by the boundaries obtained by considering all the decay channels in (i)–(iv). Some of the calculated surfaces define the decay boundary while the rest correspond to saddle points inside the decay region. Figure 2 shows an example of the decay threshold boundaries for the cubic Heisenberg antiferromagnet in applied magnetic field, the problem discussed in more detail in Sec. IV. Magnetic fields are given in units of the saturation field H_s and below $H^* \approx 0.76H_s$ decays are strictly forbidden. For $H > H^*$ the decay region grows out of the M_π point, filling out the whole Brillouin zone at $H = H_s$.

B. Decay of acoustic excitations

For a sufficiently complicated dispersion law $\varepsilon_{\mathbf{k}}$ the decay threshold boundary has to be found numerically by solving Eq. (10) and Eqs. (14)–(17). However, it is often possible to draw conclusions about the presence of decays by analyzing only the low-energy part of the spectrum. Such an approach is frequently used in theoretical studies of phonon decays (Kosevich, 2005) and we briefly review the corresponding

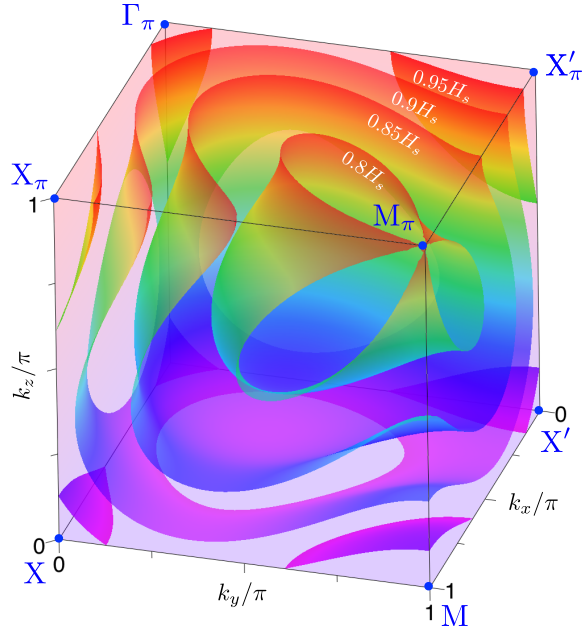


FIG. 2 (color online). Magnon decay threshold boundaries for the cubic antiferromagnet in an external field shown in one-eighth of the Brillouin zone for several values of the field. Decays are possible within the part of the Brillouin zone enclosing the M_π point.

arguments, which will also be relevant for the subsequent treatment of magnon decays.

1. Single acoustic branch

In the decay process of a long-wavelength acoustic excitation the incident and the two emitted quasiparticles have the same velocity c . The linear approximation for the excitation energy $\varepsilon_{\mathbf{k}} = ck$ does not provide sufficient information on the possibility of decays and one has to include a nonlinear correction to the linear dispersion:

$$\varepsilon_{\mathbf{k}} \approx ck + \alpha k^3. \quad (18)$$

For a weak nonlinearity $\alpha k^3 \ll ck$, the momenta of decaying and emitted quasiparticles are nearly parallel such that

$$|\mathbf{k} - \mathbf{q}| \approx k - q + \frac{kq\varphi^2}{2(k-q)}, \quad (19)$$

where φ is a small angle between \mathbf{q} and \mathbf{k} . The energy conservation (10) within the same approximation is

$$3\alpha kq(k-q) = \frac{ckq\varphi^2}{2(k-q)}. \quad (20)$$

The nontrivial solutions $q, \varphi \neq 0$ exist only for the positive sign of the cubic nonlinearity α . While the asymptotic form (18) is relevant to many physical examples, an even more general condition can be formulated to include other cases of gapless energy spectra. If the low-energy part of the spectrum is a concave function of the momentum $\partial^2\varepsilon/\partial k^2 < 0$, Fig. 3(a), magnons remain stable. On the other hand, for the upward curvature $\partial^2\varepsilon/\partial k^2 > 0$, Fig. 3(b), the low-energy excitations are unstable with respect to spontaneous decays.

Note that according to the above criterion two-magnon decays are kinematically allowed in Heisenberg ferromagnets.

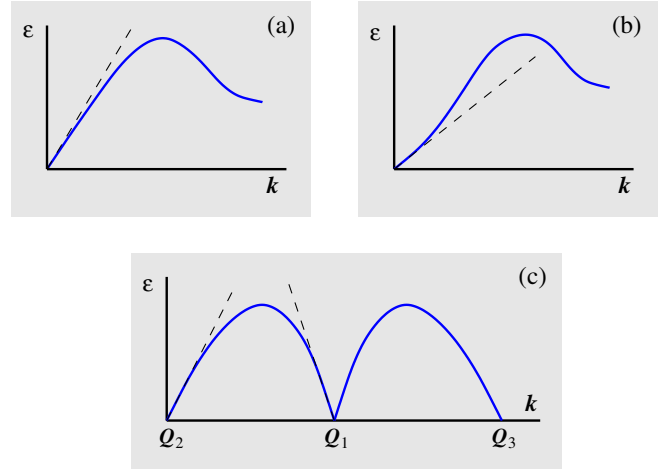


FIG. 3 (color online). Sketches of the quasiparticle spectra $\varepsilon_{\mathbf{k}}$ with (a) negative and (b) positive curvature of the acoustic mode, respectively. (c) Spectrum with several acoustic branches.

Indeed, the energy conservation equation (10) can be satisfied for quasiparticles with a ferromagnetic dispersion law $\varepsilon_{\mathbf{k}} \propto k^2$. However, as discussed in Sec. II, the decay vertices $V_3^{(1)}$ and $V_4^{(1)}$ vanish exactly in the Heisenberg ferromagnet and magnons remain well defined. Nevertheless, decays do exist in anisotropic planar ferromagnets, for which the magnon-number conservation does not hold anymore and $V_4^{(1)}$ is nonzero (Villain, 1974; Stephanovich and Zhitomirsky, 2011).

2. Several acoustic branches

Lattice vibrations in crystals have three acoustic branches with different sound velocities corresponding to one longitudinal and two transverse phonons. Heisenberg antiferromagnets with a helical or spiral magnetic structure also have three Goldstone modes, Fig. 3(c), at $\mathbf{k} = \mathbf{0}$ and $\pm\mathbf{Q}$, where \mathbf{Q} is the ordering wave vector; see Sec. V.A for more details. Energy conservation for the decay of a fast quasiparticle into two slow quasiparticles can be satisfied already in the linear approximation for the energy

$$c_1 k = c_2 q + c_3 |\mathbf{k} - \mathbf{q}|, \quad \text{for } c_1 > c_2, c_3, \quad (21)$$

where all momenta are measured relative to the corresponding Goldstone \mathbf{Q} points. Thus, if this decay channel is compatible with momentum conservation, i.e., $\mathbf{Q}_1 = \mathbf{Q}_2 + \mathbf{Q}_3$, then the fast excitation can decay regardless of the curvature of the corresponding acoustic branch.

C. Decay singularities

We now demonstrate the fact that the decay threshold boundary should generally correspond to a nonanalyticity in the particle's spectrum because of its coupling to the two-particle continuum. Consider the decay self-energy $\Sigma_a(\mathbf{k}, \omega)$ from Eq. (5) in the vicinity of the threshold boundary for two-particle decays. Generally the decay vertex has no additional smallness in terms of the momenta of participating quasiparticles, i.e., $V_3^{(1)} = \mathcal{O}(J)$. Focusing on the 2D case and expanding Eq. (10) in small $\Delta\mathbf{k} = \mathbf{k} - \mathbf{k}^*$ and $\Delta\mathbf{q} = \mathbf{q} - \mathbf{q}^*$, where \mathbf{k}^* is the crossing point of the single-magnon branch

and the bottom of the continuum and \mathbf{q}^* is the minimum point of $E_2(\mathbf{k}^*, \mathbf{q})$, energy conservation gives

$$\varepsilon_{\mathbf{k}} - \varepsilon_{\mathbf{q}} - \varepsilon_{\mathbf{k}-\mathbf{q}} \approx (\mathbf{v}_1 - \mathbf{v}_2) \cdot \Delta \mathbf{k} - \frac{\Delta q_x^2}{a^2} - \frac{\Delta q_y^2}{b^2} = 0, \quad (22)$$

where \mathbf{v}_1 and \mathbf{v}_2 are the velocities of the initial and final magnons and a and b are constants. Next, the singular part of the self-energy is given by

$$\Sigma(\mathbf{k}, \varepsilon_{\mathbf{k}}) \propto \int \frac{d^2 q}{(v_1 - v_2) \Delta k - q_x^2/a^2 - q_y^2/b^2 + i0}, \quad (23)$$

and a straightforward integration in Eq. (23) yields a logarithmic singularity in the spectrum (Zhitomirsky and Chernyshev, 1999)

$$\text{Re} \Sigma(\mathbf{k}, \varepsilon_{\mathbf{k}}) \approx \ln \frac{\Lambda}{|\Delta k|}, \quad (24)$$

$$\Gamma_{\mathbf{k}} = -\text{Im} \Sigma(\mathbf{k}, \varepsilon_{\mathbf{k}}) \approx \Theta(\Delta k),$$

where $\Theta(x)$ is the step function. The imaginary part of $\Sigma(\mathbf{k}, \varepsilon_{\mathbf{k}})$ in Eq. (7) is directly related to the two-particle density of states. Therefore, in two dimensions it is natural to have a jump in $\Gamma_{\mathbf{k}}$ upon entering the continuum, as obtained in Eq. (24). In effect this demonstrates that the van Hove singularity in the continuum's density of states gets transferred directly onto the quasiparticle spectrum via the three-particle coupling.

Consider now the other type of 2D van Hove singularity, a saddle point inside the continuum. Expansion of the energy conservation in the vicinity of the saddle point yields the same form as in Eq. (22) with a change of sign in front of either Δq_x^2 or Δq_y^2 . Therefore, the singular part of the self-energy is

$$\Sigma(\mathbf{k}, \varepsilon_{\mathbf{k}}) \propto \int \frac{d^2 q}{(v_1 - v_2) \Delta k - q_x^2/a^2 + q_y^2/b^2 + i0} \quad (25)$$

and the logarithmic singularity appears now in the imaginary part:

$$\text{Re} \Sigma(\mathbf{k}, \varepsilon_{\mathbf{k}}) \approx \text{sign}(\Delta k), \quad \Gamma_{\mathbf{k}} \approx \ln \frac{\Lambda}{|\Delta k|}, \quad (26)$$

again in agreement with the relation between the 2D two-magnon DoS and $\Gamma_{\mathbf{k}}$.

Geometric consideration of the decay surface near singularities (Chernyshev and Zhitomirsky, 2006) offers a useful alternative perspective: while crossing of the decay threshold boundary obviously corresponds to nucleation of the decay surface, the saddle-point singularity corresponds to splitting of the decay surface into two disjoint pieces. Altogether, both types of singularities (24) and (26) result from topological transitions of the decay surface with a change in the number of connected sheets.

In 3D the decay self-energy generally exhibits a less singular but still nonanalytic behavior. The logarithmic peak at the decay threshold boundary is replaced by a continuous square-root behavior $\approx \sqrt{|\Delta k|}$ for both $\text{Re} \Sigma(\mathbf{k}, \varepsilon_{\mathbf{k}})$ and $\Gamma_{\mathbf{k}}$. A remarkable exception is the threshold to the two-roton decay in the spectrum of superfluid ^4He . The dispersion

of roton excitations has a minimum on a sphere in the momentum space, leading to the same logarithmic divergence of the self-energy as in Eq. (24) at the energy twice the roton gap (Lifshitz and Pitaevskii, 1980). This strong anomaly produces the ‘‘end point’’ in the dispersion curve $\varepsilon_{\mathbf{k}}$ of the superfluid ^4He predicted by Pitaevskii (1959). Such a termination point was later observed in inelastic neutron-scattering experiments (Graf *et al.*, 1974; Glyde *et al.*, 1998).

The analysis of this section can be straightforwardly extended to the three-particle decay self-energy $\Sigma_c(\mathbf{k}, \omega)$ given by Eq. (6). The general outcome is similar to the effects of higher dimensions: singularities are replaced by continuous albeit nonanalytic behavior. Overall, the two-magnon decays play a more significant role than the higher-order decay processes. Decays and associated singularities are also enhanced by the low dimensionality of a magnetic system.

IV. FIELD-INDUCED DECAYS

We devote this section to spontaneous decays in the square-lattice Heisenberg antiferromagnet in strong external field. In zero field the ground state of this model is a two-sublattice Néel structure, which, due to its collinearity, prohibits cubic anharmonicities and two-magnon decays; see Sec. II.B. The three-magnon and all other n -magnon decays are forbidden by energy conservation, as in the cubic-lattice model studied by Harris *et al.* (1971) and in agreement with the arguments of Sec. III. Thus, in zero field and at $T = 0$ magnons have an infinite lifetime. In the opposite limit, when spins are fully polarized by an external field, the ground state is equivalent to that of a ferromagnet with all particle-nonconserving terms strictly forbidden so that the magnons are well defined again. It comes as a surprise that there exists a regime between these two limits where magnons become heavily damped throughout the Brillouin zone.

Next we discuss general arguments for the existence of the field-induced decays in a broad class of antiferromagnets and provide details of the spin-wave approach to the square-lattice antiferromagnet in a field. Focusing mostly on the $S = 1/2$ case, we demonstrate that magnons become damped and even overdamped in most of the Brillouin zone for a range of fields near the saturation field (Zhitomirsky and Chernyshev, 1999). Confirmation of these results from numerical (Syljuåsen, 2008) and experimental studies is highlighted. We also illustrate the occurrence of the threshold and saddle-point singularities discussed in Sec. III.C in the perturbative treatment of the magnon spectrum and offer two approaches to regularize them self-consistently. Detailed results of one such self-consistent regularization method (Mourigal, Zhitomirsky, and Chernyshev, 2010) are presented and an example of the higher-dimensional extension of the square-lattice case is touched upon (Fuhrman *et al.*, 2012).

A. General discussion

The evolution of an ordered magnetic structure of the two-sublattice antiferromagnet in an external field is relatively trivial. Spins orient themselves transverse to the field direction and tilt gradually toward its direction until they

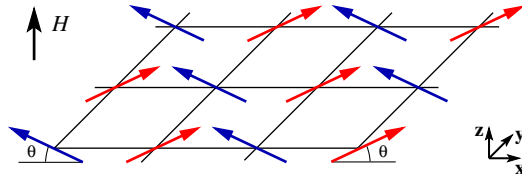


FIG. 4 (color online). Field-induced canted spin structure in the square-lattice Heisenberg antiferromagnet.

become fully aligned at $H \geq H_s$, where H_s is referred to as the saturation field; see Fig. 4. In the absence of anisotropy and frustration there is no other phase transition in the whole range from $H = 0$ to $H = H_s$. As first argued by Zhitomirsky and Chernyshev (1999), it is the dynamical properties of quantum antiferromagnets that undergo an unexpectedly dramatic transformation on the way to full saturation. The phenomenon responsible for this transformation is spontaneous magnon decay, which becomes possible in sufficiently strong magnetic fields.

The field-induced magnon decays are generally present in a broad class of quantum antiferromagnets. Indeed, three-magnon interactions that couple one- and two-magnon states always exist in canted antiferromagnetic structures created by an external field; see Sec. II. Usually, kinematic constraints prevent spontaneous decays from taking place in zero or weak magnetic fields. It is easy to see that from the acoustic branch of the magnon spectrum (18), which retains the concave shape ($\alpha < 0$) in small fields and thus is stable with respect to spontaneous decays according to Sec. III.B. However, in a strong enough magnetic field the convexity of the acoustic spectrum must change. This is because at the saturation field $H = H_s$, the magnon velocity vanishes and the dispersion at low energies is that of a ferromagnet, $\varepsilon_{\mathbf{k}} \propto k^2$, which has an upward curvature. By continuity, the spectrum has to preserve its positive curvature for a certain range of magnetic fields $H^* < H < H_s$, where the threshold field H^* corresponds to $\alpha = 0$. This implies that the two-particle decays are present at $H > H^*$.

B. Square-lattice antiferromagnet

The Heisenberg model on a square lattice, a toy model in the early days of the theory of antiferromagnets (Anderson, 1952; Kubo, 1952), became a paradigmatic model in the late 1980s due to its direct relevance to the parental materials of the high- T_c cuprates (Chakravarty, Halperin, and Nelson, 1989; Manousakis, 1991). It is also viewed as one of the prototypical strongly correlated models in condensed matter physics, used for benchmarking various theoretical methods against the more precise numerical techniques (Sandvik, 1997; White and Chernyshev, 2007).

The standard spin-wave theory provides an accurate description of the static and dynamical properties of the square-lattice antiferromagnet in zero field even for $S = 1/2$ (Hamer, Weihong, and Arndt, 1992; Igarashi, 1992; Weihong and Hamer, 1993; Igarashi and Nagao, 2005). In the words of Sandvik (1997): “The presently most accurate calculations [for the $S = 1/2$ case]... indicate that the true values of the ground-state parameters deviate from their $1/S^2$

spin-wave values by only 1–2% or less.” The spin-wave calculations also offer a fine fit to the overall magnon dispersion (Weihong and Hamer, 1993; Igarashi and Nagao, 2005; Syromyatnikov, 2010) with the only deviation from the numerical results along the $(\pi, 0)$ – $(0, \pi)$ path (Sandvik and Singh, 2001; Zheng, Oitmaa, and Hamer, 2005).

Heisenberg models in strong fields have received somewhat less attention until recently [see, however, de Jongh and Miedema (1974) and de Groot and de Jongh (1986)], primarily because the majority of available materials had exchange constants much larger than the strength of available magnetic fields. The constraints are even more stringent on neutron-scattering studies in the field, where the practical limit is currently at about 14 T. Nevertheless, recent developments in the synthesis of molecular-based antiferromagnets with moderate strength of exchange coupling between spins (Woodward *et al.*, 2002; Coomer *et al.*, 2007; Lancaster *et al.*, 2007; Xiao *et al.*, 2009) have opened the high-magnetic-field regime to experimental investigations for a number of layered square-lattice materials (Tsyulin *et al.*, 2009, 2010). Furthermore, new field-induced dynamical effects can be present in antiferromagnets with other lattice geometries (Coldea *et al.*, 2001).

Another class of antiferromagnets directly relevant to our discussion incorporates quantum spin systems with singlet ground states and gapped triplet excitations. They are often called BEC magnets because the field-induced ordering in them can be described in terms of the Bose-Einstein condensation (BEC) of triplet excitations. In recent years these quantum spin-gap magnets have been intensively studied both experimentally (Nikuni *et al.*, 2000; Jaime *et al.*, 2004; Regnault *et al.*, 2006) and theoretically (Affleck, 1991; Affleck and Wellman, 1992; Mila, 1998; Giamarchi and Tsvelik, 1999) and continue to attract attention (Giamarchi, Rugg, and Tchernyshyov, 2008). We point out that the mechanism of spontaneous magnon decays discussed here equally applies to the vicinity of the triplet condensation field H_c in these magnets because of the duality between H_c and the saturation field H_s (Mila, 1998). This is highly advantageous because in many BEC magnets the lower condensation field is readily accessible, which makes them prime candidates for observing magnon decays directly in inelastic neutron-scattering experiments. It can be argued that the recently observed suppression of thermal conductivity in the vicinity of critical fields in one such material (Kohama *et al.*, 2011) is due to magnon decays.

Extension of the spin-wave theory to finite magnetic fields was developed by Osano, Shiba, and Endoh (1982), Zhitomirsky and Nikuni (1998), Zhitomirsky and Chernyshev (1999), Chernyshev and Zhitomirsky (2009b), and Mourigal, Zhitomirsky, and Chernyshev (2010). For alternative approaches applicable in the vicinity of the saturation field, see also Batyev and Braginskii (1984), Gluzman (1993), Kreisel *et al.* (2008), and Syromyatnikov (2009). Close agreement of the spin-wave calculations with exact diagonalization and quantum Monte Carlo (QMC) results for the ground-state properties in the whole range of fields $0 < H < H_s$ was established by Lüscher and Läuchli (2009). The same work also confirmed the earlier QMC results by Syljuåsen (2008) that demonstrated clear signatures of

magnon decays in the high-field regime. We provide more details on that in the following.

1. Model and formalism

We begin with the Heisenberg Hamiltonian of nearest-neighbor spins on a square lattice in a magnetic field directed along the z_0 axis in the laboratory reference frame,

$$\hat{\mathcal{H}} = J \sum_{\langle ij \rangle} \mathbf{S}_i \cdot \mathbf{S}_j - H \sum_i S_i^{z_0}. \quad (27)$$

Here J is the nearest-neighbor coupling and H is the field in units of $g\mu_B$. With the details of the technical approach explicated by [Zhitomirsky and Nikuni \(1998\)](#) and [Mourigal, Zhitomirsky, and Chernyshev \(2010\)](#), we summarize here the key steps of the spin-wave theory approach to this problem.

First we align the local spin quantization axis on each site in the direction given by the canted spin configuration shown in Fig. 4. The corresponding transformation of the spin components from the laboratory frame (x_0, y_0, z_0) to the local frame is

$$\begin{aligned} S_i^{x_0} &= S_i^x \sin\theta + S_i^z e^{i\mathbf{Q}\cdot\mathbf{r}_i} \cos\theta, & S_i^{y_0} &= S_i^y, \\ S_i^{z_0} &= -S_i^x e^{i\mathbf{Q}\cdot\mathbf{r}_i} \cos\theta + S_i^z \sin\theta, \end{aligned} \quad (28)$$

where θ is the canting angle to be defined from the energy minimization and $\mathbf{Q} = (\pi, \pi)$ is the ordering wave vector of the two-sublattice Néel structure. Next the standard Holstein-Primakoff transformation bosonizes the spin operators $S_i^z = S - a_i^\dagger a_i$, $S_i^- = a_i^\dagger (2S - a_i^\dagger a_i)^{1/2}$, with $S_i^\pm = S_i^x \pm iS_i^y$. Expanding square roots, one obtains the bosonic Hamiltonian as a sum,

$$\hat{\mathcal{H}}_{\text{SW}} = \hat{\mathcal{H}}_0 + \hat{\mathcal{H}}_1 + \hat{\mathcal{H}}_2 + \hat{\mathcal{H}}_3 + \hat{\mathcal{H}}_4 + \dots, \quad (29)$$

each term being of the n th order in the bosonic operators a_i^\dagger and a_i and carrying an explicit factor $S^{2-n/2}$. This form provides the basis for the $1/S$ expansion. Important consequences of the noncollinear spin structure are the terms $S_j^z S_i^{x(y)}$, which describe coupling between transverse $S^{x(y)}$ and longitudinal S^z oscillations and yield cubic anharmonicities ($\hat{\mathcal{H}}_3$) in the bosonic Hamiltonian.

Minimization of the classical energy $\hat{\mathcal{H}}_0$ in Eq. (29) fixes the canting angle of the classical spin structure to $\sin\theta = H/H_s$, where the saturation field is $H_s = 8JS$. This procedure also cancels the $\hat{\mathcal{H}}_1$ term that is linear in a_i^\dagger and a_i . After subsequent Fourier transformation, the harmonic part of the Hamiltonian ($\hat{\mathcal{H}}_2$) is diagonalized by the Bogolyubov transformation $a_{\mathbf{k}} = u_{\mathbf{k}} b_{\mathbf{k}} + v_{\mathbf{k}} b_{-\mathbf{k}}^\dagger$, yielding

$$\begin{aligned} \hat{\mathcal{H}}_{\text{SW}} &= \sum_{\mathbf{k}} \tilde{\varepsilon}_{\mathbf{k}} b_{\mathbf{k}}^\dagger b_{\mathbf{k}} \\ &+ \frac{1}{2} \sum_{\mathbf{k}, \mathbf{q}} V_3^{(1)}(\mathbf{k}, \mathbf{q}) (b_{\mathbf{k}-\mathbf{q}}^\dagger b_{\mathbf{q}}^\dagger b_{\mathbf{k}} + \text{H.c.}) + \dots, \end{aligned} \quad (30)$$

where $\tilde{\varepsilon}_{\mathbf{k}} = \varepsilon_{\mathbf{k}} + \delta\varepsilon_{\mathbf{k}}$, with $\varepsilon_{\mathbf{k}}$ being the magnon dispersion given by the linear spin-wave theory and $\delta\varepsilon_{\mathbf{k}}$ is from the $1/S$ corrections due to angle renormalization and Hartree-Fock decoupling of cubic and quartic terms in Eq. (29),

respectively. The ellipsis stands for the classical energy, the three-boson source term $V_3^{(2)}$ as in Eq. (3), and the higher-order terms in the $1/S$ expansion. Although some of these terms do contribute to the subsequent results, this abbreviated form constitutes the essential part of the Hamiltonian and is sufficient for our discussion. For the explicit expressions of $\delta\varepsilon_{\mathbf{k}}$ and vertices $V_3^{(1)}$ and $V_3^{(2)}$, see [Mourigal, Zhitomirsky, and Chernyshev \(2010\)](#).

2. Decay region

One can already gain detailed insight into the decay conditions in the manner discussed in Sec. III by analyzing the magnon spectrum in the harmonic approximation, which is given by

$$\varepsilon_{\mathbf{k}} = 4JS\sqrt{(1 + \gamma_{\mathbf{k}})(1 - \cos 2\theta\gamma_{\mathbf{k}})}, \quad (31)$$

where $\gamma_{\mathbf{k}} = \frac{1}{2}(\cos k_x + \cos k_y)$. The acoustic mode near \mathbf{Q} follows the asymptotic form (18) $\varepsilon_{\mathbf{Q}+\mathbf{k}} \approx ck + \alpha k^3$ with

$$c = 2\sqrt{2}JS\cos\theta, \quad \alpha = \frac{c}{16} \left(\tan^2\theta - \frac{9 + \cos 4\varphi}{6} \right), \quad (32)$$

where φ is the azimuthal angle of $\mathbf{k} = (k_x, k_y)$. The curvature of the spectrum α changes its sign for \mathbf{k} along the diagonal ($\varphi = \pi/4$) at the decay threshold field

$$H^* = \frac{2}{\sqrt{7}} H_s \approx 0.7559 H_s. \quad (33)$$

Note that this expression remains valid for the cubic- and for the layered square-lattice antiferromagnet with arbitrary antiferromagnetic interlayer coupling.

Staggered canting of spins in Eq. (28) ‘‘shifts’’ the momentum in the two-magnon decay condition in Eq. (10), which now reads as $\varepsilon_{\mathbf{k}} = \varepsilon_{\mathbf{q}} + \varepsilon_{\mathbf{k}-\mathbf{q}+\mathbf{Q}}$. Using the Bose-condensate perspective of Sec. II.B, such a change is natural as the magnon going into the condensate now carries the momentum \mathbf{Q} ; see Eq. (4). Apart from that the kinematic analysis of Sec. III remains the same. Numerical results for the decay region at $H > H^*$ are shown in Fig. 5. Up to $H \approx 0.84H_s$ the boundary of the decay region is determined entirely by the decays into a pair of magnons with equal

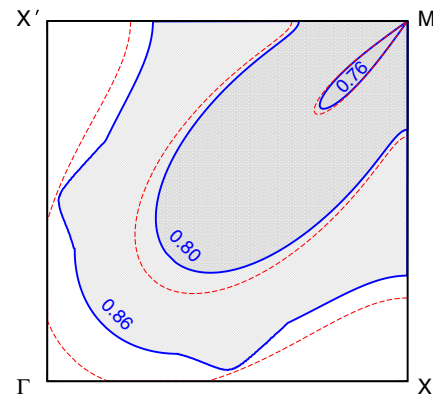


FIG. 5 (color online). Decay regions in one-fourth of the Brillouin zone for representative values of H/H_s indicated by numbers. Solid and dashed lines are threshold boundaries for two- and three-magnon decays, respectively.

momenta; see Sec. III.A, type (i) in Eq. (15). At fields higher than $0.85H_s$ the decay channel with emission of an acoustic magnon, type (ii) in Eq. (16), creates protrusions leading to more complicated shapes of the decay region. Above $0.9H_s$ the decay region spreads almost over the entire Brillouin zone, similarly to the 3D decay regions in Fig. 2. In Fig. 5, we also show boundaries for the three-magnon decays, which are less restrictive and cover larger areas of the Brillouin zone than their two-magnon counterparts.

C. Spectral function and self-consistent Born approximation

Information on the magnon energy renormalization and decay-induced lifetime due to interactions can be obtained from the single-particle spectral function $A(\mathbf{k}, \omega) = -(1/\pi) \text{Im}G(\mathbf{k}, \omega)$. Here $G(\mathbf{k}, \omega)$ is the interacting Green's function

$$G^{-1}(\mathbf{k}, \omega) = \omega - \tilde{\epsilon}_{\mathbf{k}} - \Sigma_a(\mathbf{k}, \omega) - \Sigma_b(\mathbf{k}, \omega), \quad (34)$$

where $\Sigma_{a,b}(\mathbf{k}, \omega)$ are the decay and source self-energies shown in Fig. 1, with the ‘‘one-loop’’ expressions for them given in Eq. (5). Importantly, the magnon spectral function is directly related to the dynamical structure factor $S(\mathbf{k}, \omega)$ measured in neutron-scattering experiments; see Mourigal, Zhitomirsky, and Chernyshev (2010) for the details of their connection.

The self-energies in Eq. (34) originate from coupling to the two-magnon continuum, and already in the lowest order one expects the spectral function to exhibit an incoherent component due to two-magnon states in addition to the quasiparticle peak that is broadened due to decays. The Born approximation (BA) results for $A(\mathbf{k}, \omega)$ for several momenta along the ΓM line at $H = 0.9H_s$ are shown in Fig. 6 by dashed lines. While $A(\mathbf{k}, \omega)$ exhibits incoherent subbands, the peaks survive even for \mathbf{k} deep inside the decay region in Fig. 8. This is due to the lack of self-consistency in the lowest-order BA, as one- and two-magnon states are treated with different accuracy. Specifically, the magnon energy is renormalized

downward by the real part of $\Sigma_{a,b}(\mathbf{k}, \omega)$ in Eq. (34), whereas the energy of the continuum is still calculated in the harmonic approximation. Taking into account energy renormalization of the continuum means ‘‘dressing’’ of the inner lines of the decay diagram in Fig. 1. The main technical difficulty with such a self-consistent Born approximation (SCBA) is that it opens an unphysical gap for long-wavelength magnons, in violation of the Goldstone theorem.

This difficulty notwithstanding, the restricted SCBA scheme was implemented by Zhitomirsky and Chernyshev (1999), which included partial renormalization of the two-magnon continuum. It enforced the acoustic form of the long-wavelength magnon dispersion (18) and incorporated the self-consistent renormalization of one inner magnon line in the decay diagram of Fig. 1(a). The results of the numerical solution of Dyson's equation in the restricted SCBA are shown in Fig. 6 by solid lines. Not only are the peaks that were artifacts of the non-self-consistent treatment completely wiped out, but the overall values of magnon damping are large away from the \mathbf{Q} and Γ points, the latter corresponding to the uniform precession mode which is stable.

These results received strong confirmation from the numerical QMC simulations by Syljuåsen (2008) (see Fig. 7), and, subsequently, from the exact diagonalization (ED) study by Lüscher and Läuchli (2009). Both numerical works found significant modifications in the magnon spectra above the threshold field: an explicit broadening of peaks in the dynamical structure factor revealed by QMC data and a qualitative transformation in the structure of energy levels and in distribution of spectral weights observed in ED. Figure 7 shows the intensity plot of the $S^{zz}(\mathbf{q}, \omega)$ component of the dynamical structure factor from Syljuåsen (2008). Since $S^{zz}(\mathbf{q}, \omega)$ is proportional to the spectral function with a shifted momentum $A(\mathbf{q} - \mathbf{Q}, \omega)$ (Fuhrman *et al.*, 2012), gapless and uniform precession modes trade their places in Fig. 7.

There are close qualitative and quantitative similarities between the analytical and numerical results of Figs. 6 and 7. Magnon decays and spectrum broadening are strongly

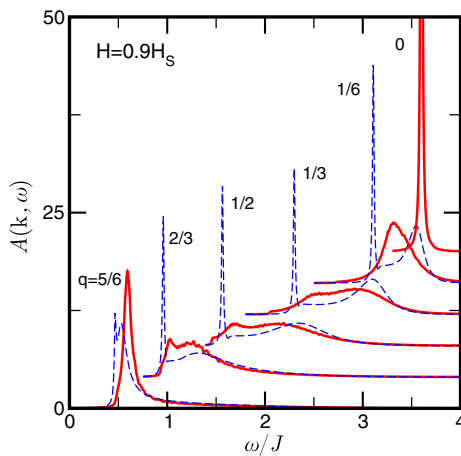


FIG. 6 (color online). Magnon spectral function for the spin- $\frac{1}{2}$ antiferromagnet at $H = 0.9H_s$ for $\mathbf{k} = \pi(q, q)$. Dashed and solid lines correspond to Born approximation and restricted self-consistent born approximation, respectively. From Zhitomirsky and Chernyshev, 1999.

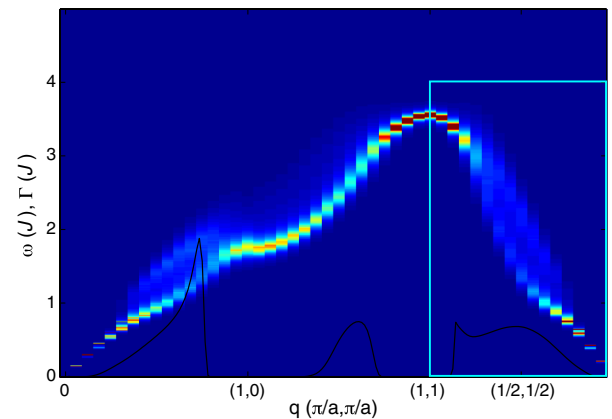


FIG. 7 (color online). QMC results for the $S^{zz}(\mathbf{q}, \omega)$ component of the dynamical structure factor for the $S = 1/2$ square-lattice antiferromagnet at $H = 0.875H_s$ along the $\Gamma XM\Gamma$ path. Black lines are the magnon linewidths in the Born approximation (Syljuåsen, 2008). The box marks the \mathbf{k} - ω region of Fig. 6 for comparison. From Olav Syljuåsen, 2008.

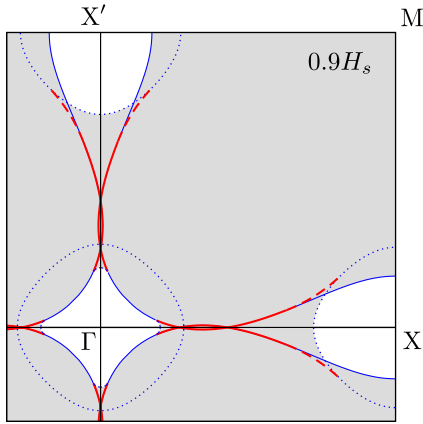


FIG. 8 (color online). Decay region and associated singularities for $H = 0.9H_s$. Solid, dashed, and dotted lines denote the decay channels into a pair of magnons with equal momenta and different momenta, and emission of an acoustic magnon, respectively. Thick portions of solid and dashed lines indicate the saddle-point singularity in the continuum, while the thin parts correspond to local minima.

pronounced and follow decay regions suggested by the kinematic analysis of Sec. IV.B. Syljuåsen also emphasized the nontrivial redistribution of spectral weight resulting in non-Lorentzian “double-peak” features in the dynamical structure factor, also seen in the analytical results in Fig. 6, albeit less pronounced. In spite of the approximations of the analytical approach and of the uncertainties in the QMC results due to numerical interpolation from imaginary to real frequencies, such a correspondence between two very different methods is truly remarkable.

Following the original prediction of the field-induced spontaneous magnon decays, there is an ongoing search for suitable spin- $\frac{1}{2}$ square-lattice materials (Coomer *et al.*, 2007; Lancaster *et al.*, 2007; Tsyulin *et al.*, 2009) to investigate corresponding effects. Recently, Masuda *et al.* (2010) found indications of the field-induced decays in the inelastic neutron-scattering spectra of the spin- $\frac{5}{2}$ layered square-lattice antiferromagnet $\text{Ba}_2\text{MnGe}_2\text{O}_7$.

D. Decay singularities and SCBA

While the preceding consideration demonstrates the spectacular role of spontaneous decays in reshaping the magnon spectrum in the high-field regime of the $S = 1/2$ square-lattice antiferromagnet, several aspects of the bigger picture remain unclear. In particular, what about the threshold and saddle-point singularities discussed in Sec. III? Are there termination points in the magnon spectrum? How strong is the magnon damping in more quasiclassical $S \geq 1$ systems? These questions were addressed recently by Mourigal, Zhitomirsky, and Chernyshev (2010).

First we substantiate the generic analysis of the threshold singularities provided in Sec. III by giving a specific example from the square-lattice antiferromagnet. In Fig. 8 we show the decay region for $H = 0.9H_s$ together with the set of contours obtained by the analysis of Sec. III.A. The solid, dashed, and dotted lines are the singularity contours for the decay into

magnons with the same (15) and different momenta, and for the emission of an acoustic magnon (16), respectively. Line thickness indicates a singularity that corresponds to a minimum (saddle point) of the continuum. The same singularity contour may correspond to a minimum in one part of the Brillouin zone and to a saddle point in the other. This determines whether the logarithmic singularity will occur in the real or imaginary part of the self-energy, as discussed in Sec. III.C.

Within the spin-wave expansion, the $1/S$ renormalization for the magnon spectrum is given by

$$\bar{\varepsilon}_{\mathbf{k}} = \tilde{\varepsilon}_{\mathbf{k}} + \text{Re}\Sigma_a(\mathbf{k}, \varepsilon_{\mathbf{k}}) + \Sigma_b(\mathbf{k}, \varepsilon_{\mathbf{k}}), \quad (35)$$

where $\tilde{\varepsilon}_{\mathbf{k}} = \varepsilon_{\mathbf{k}} + \delta\varepsilon_{\mathbf{k}}$ already contains the Hartree-Fock corrections to the linear spin-wave dispersion $\varepsilon_{\mathbf{k}}$ [see Eq. (30)], and the magnon damping is $\Gamma_{\mathbf{k}} = -\text{Im}\Sigma_a(\mathbf{k}, \varepsilon_{\mathbf{k}})$ in the same approximation. In Fig. 9 we present numerical results for the renormalized magnon energy and damping for $H = 0.9H_s$, $S = 1/2$, and for \mathbf{k} along the $M\Gamma X$ line, which crosses several threshold boundaries according to Fig. 8. The magnon energy exhibits singularities that are clearly related to spontaneous magnon decays: every spike or jump in $\bar{\varepsilon}_{\mathbf{k}}$ is accompanied by a jump or a peak in the decay rate $\Gamma_{\mathbf{k}}$. In agreement with Sec. III.C, the logarithmic singularities occur on a crossing of the singularity contour with substantial density of two-magnon states, a minimum or a saddle point of the continuum outlined in Fig. 8.

Such singularities invalidate the usual $1/S$ expansion because the renormalized spectrum contains divergences. The encountered problem is generic and must be common to a variety of the 2D models regardless of the value of the on-site spin S . For systems with large spin the situation is especially aggravating as the $1/S$ expansion changes from a reliable approach to one producing unphysical divergences, undermining any sensible comparison with experimental or numerical data.

Singular corrections to the spectrum obtained in the leading order require a higher-order regularization, which depends on the form of $\varepsilon_{\mathbf{k}}$. For example, two-roton decay in the superfluid ^4He yields logarithmic divergence of the one-loop diagram in Fig. 1(a) near the decay threshold. Using regularization of the two-particle scattering amplitude,

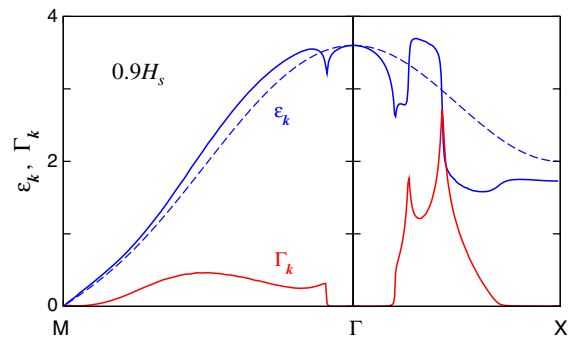


FIG. 9 (color online). Magnon energy and decay rate in units of J for the spin- $\frac{1}{2}$ square-lattice antiferromagnet along the $M\Gamma X$ path at $H = 0.9H_s$. The two upper curves show the harmonic $\varepsilon_{\mathbf{k}}$, dashed line, and the renormalized magnon energy $\bar{\varepsilon}_{\mathbf{k}}$, solid line. The lower curve gives the decay rate $\Gamma_{\mathbf{k}}$.

Pitaevskii (1959) showed that such thresholds become termination points of the spectrum; this was later confirmed experimentally (Glyde *et al.*, 1998). However, this salient feature of the ^4He spectrum is owing to the form of $\varepsilon_{\mathbf{k}}$, which ensures that rotons created in the decay process are well defined. The problem considered here is qualitatively different because magnons created in an elementary decay are also unstable. This can be seen from the evolution of the decay regions versus field in Fig. 5, which begins with the acoustic branch where the typical decay processes produce magnons further within that region.

Such ‘‘cascade’’ decays imply the following. First, the threshold and saddle-point singularities in Eqs. (24) and (26) are removed by changing $|\Delta k| \rightarrow \sqrt{(\Delta k)^2 + (\Gamma_{q^*}/c_{q^*})^2}$, where Γ_{q^*} is the damping of the ‘‘singular’’ decay products and c_{q^*} is related to their velocities (Mourigal, Zhitomirsky, and Chernyshev, 2010). Second, the higher-order regularization treatment must include damping of the decay products. Thus, as in Sec. IV.C, dressing of the bare propagators in Fig. 1(a) within the SCBA should yield a regularized spectrum. Having in mind the technical difficulty of this approach we used instead another scheme, referred to as imaginary-part SCBA (iSCBA). This treats the magnon decay rate $\Gamma_{\mathbf{k}}$ self-consistently, but neglects quantum corrections to $\varepsilon_{\mathbf{k}}$ altogether (Mourigal, Zhitomirsky, and Chernyshev, 2010). Indeed, away from singularities and for larger spins $S \geq 1$, renormalization of the spectrum $\delta\varepsilon_{\mathbf{k}} \sim \mathcal{O}(J)$ is small compared to the bare energy $\varepsilon_{\mathbf{k}} \sim \mathcal{O}(SJ)$ and can be neglected. Although the intrinsic damping is of the same order $\Gamma_{\mathbf{k}} \sim \mathcal{O}(J)$, it represents the most important qualitatively new feature of the spectrum acquired due to spontaneous decays.

In the simplest realization of the iSCBA we impose the following ansatz on the Green’s function:

$$G^{-1}(\mathbf{k}, \omega) = \omega - \varepsilon_{\mathbf{k}} + i\Gamma_{\mathbf{k}}. \quad (36)$$

This approximation is equivalent to assuming a Lorentzian shape of the quasiparticle peaks in the dynamical response. Neglecting contributions from the source diagram, the self-consistent equation for the magnon decay rate $\Gamma_{\mathbf{k}}$ becomes

$$\Gamma_{\mathbf{k}} = \frac{1}{2} \sum_{\mathbf{q}} \frac{|V_3^{(1)}(\mathbf{q}; \mathbf{k})|^2 (\Gamma_{\mathbf{q}} + \Gamma_{\mathbf{k}-\mathbf{q}+\mathbf{Q}})}{(\varepsilon_{\mathbf{k}} - \varepsilon_{\mathbf{q}} - \varepsilon_{\mathbf{k}-\mathbf{q}+\mathbf{Q}})^2 + (\Gamma_{\mathbf{q}} + \Gamma_{\mathbf{k}-\mathbf{q}+\mathbf{Q}})^2}. \quad (37)$$

Such a scheme was previously applied to the problem of phonon damping in ^4He (Sluckin and Bowley, 1974) and in quasicrystals (Kats and Muratov, 2005).

One of the qualitative results of the iSCBA approach can be immediately anticipated: since by dressing the diagram in Fig. 1(a) we implicitly take into account all n -particle decay processes, the \mathbf{k} region where magnons are damped is no longer confined to the two-magnon decay region. In Fig. 5 we provide an indication of that by showing the decay regions for the three-magnon processes (dashed lines). These are generally weaker than the leading two-magnon decays, but their kinematics is less restrictive as for any given $H > H^*$ the two-magnon decay area in Fig. 5 is enclosed by the three-magnon one. In the limit of $n \rightarrow \infty$, the decay region extends farther

and can cover the entire Brillouin zone in the high-field regime.

The same conclusion is reached if we consider broadening of the decay threshold singularity by the finite lifetime of the final-state magnons. This broadening implies that the boundary in the momentum space between stable and damped magnons is smeared out and the decay probability disappears gradually rather than in a steplike fashion.

The numerical solution of the iSCBA Eq. (37) for two representative values of spin $S = 1$ and $S = 5/2$ and for several field values is presented in Fig. 10 in the form of intensity maps of $\Gamma_{\mathbf{k}}/4JS$ vs \mathbf{k} in the same part of the Brillouin zone as in Fig. 8. As discussed, the singularities in $\Gamma_{\mathbf{k}}$ are washed out and finite damping develops outside of the original decay regions of Figs. 5 and 8. Comparison of the upper ($S = 1$) and lower ($S = 5/2$) rows in Fig. 10 reveals similar patterns in the momentum distribution of $\Gamma_{\mathbf{k}}$.

Specifically, in lower fields, $H \lesssim 0.9H_s$, magnon damping is most significant in the broad region around the $(\pi/2, \pi/2)$ point, which is a consequence of the large phase-space volume for the two-particle decays in this region. In higher fields, the maxima in the decay rate shift to the ΓX ($\Gamma X'$) lines where the enhancement of damping is due to the remnants of the strong logarithmic saddle-point singularities in Fig. 9. For $S \gg 1$ one can show that $\Gamma_{\mathbf{k}} \sim \mathcal{O}(J)$ away from the former singular contours but there is a parametric enhancement of damping $\Gamma_{\mathbf{k}} \sim \mathcal{O}(J \ln S)$ in their vicinity (Chernyshev and Zhitomirsky, 2009a).

To summarize, the self-consistently calculated magnon damping in the large- S square-lattice antiferromagnet in strong fields is free from singularities and does not exceed $\Gamma_{\mathbf{k}}^{\max} \sim 0.7J - 0.8J$. In other words, spin waves in large- S systems acquire finite lifetimes at $H > H^*$ but remain well-defined quasiparticles. The regularized singularities lead to a parametric enhancement of magnon damping and produce distinct field dependence and momentum dependence of $\Gamma_{\mathbf{k}}$. The above results are in qualitative agreement with the inelastic neutron-scattering data on the spin- $\frac{5}{2}$ layered square-lattice antiferromagnet $\text{Ba}_2\text{MnGe}_2\text{O}_7$ (Masuda *et al.*, 2010), although more refined measurements are

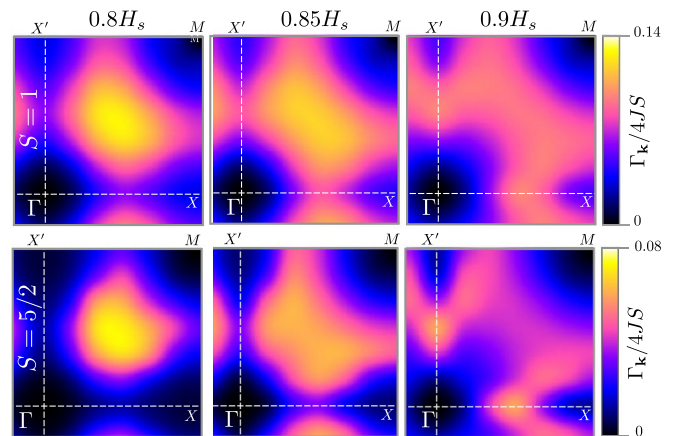


FIG. 10 (color online). Intensity maps of the magnon decay rate $\Gamma_{\mathbf{k}}$ calculated within the iSCBA for several values of external magnetic field and for two values of the spin: $S = 1$ (upper panels) and $S = 5/2$ (lower panels).

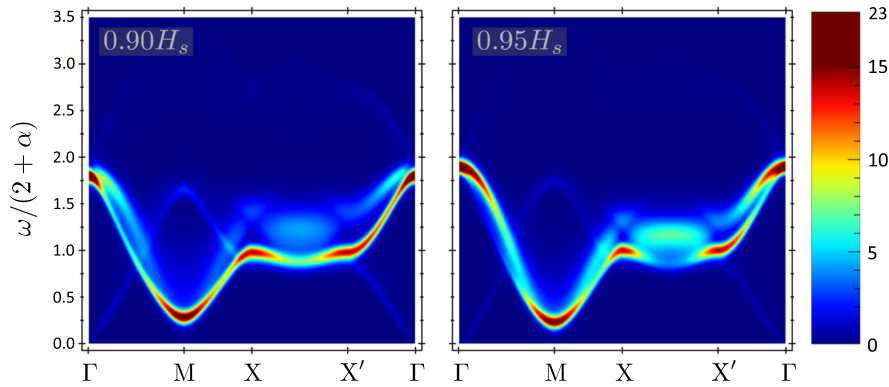


FIG. 11 (color online). Intensity plots of the dynamical structure factor $S(\mathbf{k}, \omega)$, for fields $0.9H_s$ and $0.95H_s$, $S = 1/2$, and for the \mathbf{k} path in the $k_z = 0$ plane, along the $\Gamma \rightarrow M \rightarrow X \rightarrow X' \rightarrow \Gamma$ line; see Fig. 2 for notations. From Fuhrman *et al.*, 2012.

necessary for a detailed comparison between theory and experiment.

E. Decays in three dimensions

In the two preceding sections we presented results of self-consistent schemes that dealt with the unrealistic escape of the quasiparticle peaks from the unrenormalized two-magnon continuum and with singularities encountered in the $1/S$ expansion. However, as noted in Sec. III.C, the decay-induced divergencies in $\Gamma_{\mathbf{k}}$ and $\bar{\epsilon}_{\mathbf{k}}$ in 2D are replaced by a continuous albeit nonanalytic behavior in 3D. Recent work by Fuhrman *et al.* (2012) demonstrated that a moderate interlayer coupling mitigates 2D singularities and represents an alternative to the above self-consistency schemes. This approach allows one to obtain the excitation spectrum using the standard spin-wave expansion, without the use of self-consistency, with no restrictions on the spectral shapes and at a fraction of the computational cost. As a specific example, we calculated the dynamical structure factor of the quasi-2D $S = 1/2$ square-lattice antiferromagnet with moderate interlayer coupling $J'/J = 0.2$, which is relevant to one of the prospective materials for observing magnon decays, $(5\text{CAP})_2\text{CuCl}_4$, where 5CAP is 2-amino-5-chloropyridinium (Coomer *et al.*, 2007).

In Fig. 11, we show these results in the form of intensity plots of the dynamical structure factor $S(\mathbf{k}, \omega)$ for $H = 0.9H_s$ and $0.95H_s$ along a representative path in the Brillouin zone; see Fig. 2 for notations and Fuhrman *et al.* (2012) for details. In addition to the main features that are directly related to the magnon spectral function $A(\mathbf{k}, \omega)$, the out-of-plane transverse mode contribution is visible as a shadow, shifted by the ordering vector $\mathbf{Q} = (\pi, \pi, \pi)$. We performed a Gaussian convolution in the ω direction with a σ width of $0.1J$. This step is intended to mimic the effect of a realistic experimental resolution, from which we can also draw quantitative predictions of the relative strength of the quasiparticle and the incoherent part of the spectrum.

Complex spectral line shapes, very much distinct from the conventional quasiparticle peaks, are clearly visible in Fig. 11. This demonstrates that the effects of spectral weight redistribution and broadening due to spontaneous decays are

substantial and should be readily observed in experiment. The structure factor exhibits a variety of unusual features, including the double-peak line shape for the ΓM direction discussed previously. Along some of the \mathbf{k} directions for $H = 0.9H_s$, the renormalized quasiparticle peaks escape the unrenormalized two-magnon continuum and survive despite being formally within the decay region shown in Fig. 2. Yet these peaks are accompanied by continuumlike subbands that accumulate significant weight. Upon increase of the field, the continuum overtakes the single-particle branches in large regions of the Brillouin zone, washing them out and creating more double-peak structures, e.g., very distinctly along the $X\Gamma$ direction. There is a particularly spectacular advance of the continuum along the XX' line, where magnon broadening is most intense, with dramatic spectral weight transfer to higher energies.

The overall landscape of the high-field dynamical structure factor shown here is diverse and intriguing. Our results, consistent with prior numerical and analytical studies, provide a comprehensive illustration of its details. Inelastic neutron-scattering measurements on suitable quantum antiferromagnets will be important to elucidate the accuracy of our theoretical results.

V. ZERO-FIELD DECAYS

In this section we discuss spontaneous decays in noncollinear antiferromagnets in zero magnetic field. As explained in Sec. II, the noncollinear magnetic structures necessarily lead to the coupling of transverse and longitudinal spin fluctuations that translates into cubic anharmonicities in the effective magnon Hamiltonian. This opens the door to spontaneous two-magnon decays without the assistance of an external field, provided the kinematic conditions of Sec. III are fulfilled. Here we concentrate on the case of *spiral* Heisenberg antiferromagnets, in which the noncollinear ground state spontaneously breaks the $\text{SO}(3)$ symmetry of the spin Hamiltonian. We show that the kinematic conditions that allow two-magnon decays are always fulfilled in such a case, owing to the existence of three acoustic branches in the excitation spectra. Next we elucidate these features and consider magnon decays in the spin- $\frac{1}{2}$ triangular-lattice antiferromagnet in more detail.

Our subsequent discussion does not include noncollinear magnetic structures induced by the anisotropic Dzyaloshinskii-Moriya interactions, which have attracted a lot of interest because of experimental observation of the skyrmion lattices (Röblier, Bogdanov, and Pfleiderer, 2006). We also leave aside the other cases of noncollinear antiferromagnets, such as kagomé-lattice potassium jarosite (Matan *et al.*, 2006) and anisotropic triangular-lattice antiferromagnets, discussed by Chernyshev and Zhitomirsky (2009a), although many qualitative aspects of our consideration below remain valid for them. Yet another class of zero-field spontaneous decays that do not require noncollinearity, the three-magnon decays in anisotropic ferromagnets (Villain, 1974; Stephanovich and Zhitomirsky, 2011), is also left out.

A. General discussion

Noncollinear spin structures in isotropic antiferromagnets appear as a consequence of magnetic frustration: either because of the geometry of the nearest-neighbor bonds as, e.g., for a triangular lattice, or due to competing exchange interactions beyond the nearest-neighbor shell. Here we consider a general case of the Heisenberg Hamiltonian

$$\hat{\mathcal{H}} = \sum_{\langle ij \rangle} J(\mathbf{r}) \mathbf{S}_i \cdot \mathbf{S}_j, \quad (38)$$

where spins occupy the sites of a Bravais lattice and $\mathbf{r} \equiv \mathbf{r}_j - \mathbf{r}_i$. The lowest-energy classical state of this model is a spin helix with a wave vector \mathbf{Q} , which is found by minimizing the Fourier transform of the exchange energy $J_{\mathbf{q}} = \sum_{\mathbf{r}} J(\mathbf{r}) \cos(\mathbf{q} \cdot \mathbf{r})$.

The spin-wave theory has been applied to spiral magnetic structures in a number of works; see, for example, Chubukov (1984) and Ohyama and Shiba (1993). Similarly to the procedure discussed in Sec. IV.B, the classical spin configuration defines the rotating local basis for spin quantization, which is related to the laboratory frame via

$$\begin{aligned} S_i^{x_0} &= S_i^z \sin \mathbf{Q} \cdot \mathbf{r}_i + S_i^x \cos \mathbf{Q} \cdot \mathbf{r}_i, & S_i^{y_0} &= S_i^y, \\ S_i^{z_0} &= S_i^z \cos \mathbf{Q} \cdot \mathbf{r}_i - S_i^x \sin \mathbf{Q} \cdot \mathbf{r}_i. \end{aligned} \quad (39)$$

The subsequent $1/S$ expansion follows standard steps (see Sec. IV.B) and yields the spin-wave dispersion in the harmonic approximation:

$$\varepsilon_{\mathbf{k}} = S \sqrt{(J_{\mathbf{k}} - J_{\mathbf{Q}}) \left(\frac{1}{2} J_{\mathbf{Q}+\mathbf{k}} + \frac{1}{2} J_{\mathbf{Q}-\mathbf{k}} - J_{\mathbf{Q}} \right)}. \quad (40)$$

One can see that for an arbitrary form of $J_{\mathbf{q}}$ the excitation energy vanishes at three wave vectors: $\mathbf{k} = \mathbf{0}$ and $\pm \mathbf{Q}$. The existence of these three Goldstone modes follows from the complete breaking of the rotational $\text{SO}(3)$ symmetry in the noncollinear ground state (Andreev and Marchenko, 1980; Dombre and Read, 1989). For a planar magnetic structure, spin waves with $\mathbf{k} = \pm \mathbf{Q}$ correspond to the out-of-plane oscillation modes related by symmetry, whereas the $\mathbf{k} = \mathbf{0}$ mode represents the in-plane oscillations of the spin spiral. Overall there are three acoustic branches, shown schematically in Fig. 3(c), with two distinct spin-wave velocities c_0 and c_Q .

As was noted, coupling between one- and two-magnon states is inevitable in noncollinear structures. Hence, to verify the presence or absence of spontaneous decays in spiral antiferromagnets one only needs to analyze the kinematic constraints following from the energy conservation (10). Our discussion in Sec. III.B suggests that in a system with multiple acoustic modes the fast low-energy magnons can always decay into slow ones. Using Eq. (40) one can obtain the velocities of the two acoustic modes as

$$\begin{aligned} c_0 &= S \sqrt{A(J_0 - J_{\mathbf{Q}})}, & A &= \frac{1}{2} \nabla_{\mathbf{k}}^2 J_{\mathbf{k}} \big|_{\mathbf{k}=\mathbf{Q}}, \\ c_Q &= S \sqrt{A \left(\frac{1}{2} J_0 + \frac{1}{2} J_{2\mathbf{Q}} - J_{\mathbf{Q}} \right)}. \end{aligned} \quad (41)$$

Since the ordering wave vector of a spiral structure has to satisfy the inequality $2\mathbf{Q} \neq \mathbf{G}_i$, the \mathbf{G}_i 's being reciprocal lattice vectors, the two velocities in Eq. (41) are generally different. If $J_0 > J_{2\mathbf{Q}}$, the in-plane mode is faster: $c_0 > c_Q$. For example, this relation holds if all exchange constants are antiferromagnetic, $J(\mathbf{r}) > 0$. In such a case the decay channel $\mathbf{k} \rightarrow (\mathbf{Q} + \mathbf{q}) + (-\mathbf{Q} + \mathbf{q}')$ is always open for sufficiently small \mathbf{k} . Since for the linearized spectra decays would be permitted for any \mathbf{k} , it is the short-range behavior of $J_{\mathbf{q}}$ that limits the size of the decay region, which typically occupies an extended region of the Brillouin zone including the Γ point. Generally, acoustic branches emanating from the $\pm \mathbf{Q}$ points remain undamped for an incommensurate \mathbf{Q} , although, see the discussion of the triangular-lattice case in Sec. V.B. If, on the other hand, $J_0 < J_{2\mathbf{Q}}$, which happens when some bonds are ferromagnetic, out-of-plane modes are faster: $c_0 < c_Q$. Now the decay channel is switched to $(\mathbf{Q} + \mathbf{k}) \rightarrow (\mathbf{Q} + \mathbf{q}) + \mathbf{q}'$ for small \mathbf{k} such that the decay region surrounds the $\pm \mathbf{Q}$ points, while magnons in the center of the Brillouin zone remain undamped.

In this discussion we disregarded possible anisotropy of the spin-wave velocities. However, since both c_0 and c_Q have the same angular dependence via A in Eq. (41), the anisotropy plays only a secondary role, which does not change the qualitative conclusion about the magnon decay region.

A finite lifetime of magnetic excitations was noted in several studies of noncollinear antiferromagnets within the higher-order spin-wave theory (Ohyama and Shiba, 1993; Veillette, James, and Essler, 2005; Dalidovich *et al.*, 2006; Strykh, Chubukov, and Abanov, 2006). The generality of the phenomenon of spontaneous magnon decays in spiral antiferromagnets was emphasized in our work (Chernyshev and Zhitomirsky, 2006), in which we studied in detail the triangular-lattice Heisenberg antiferromagnets considered next.

B. Triangular-lattice antiferromagnet

The semiclassical $S \gg 1$ triangular-lattice antiferromagnet orders in the 120° spin structure shown in Fig. 12. For the case of $S = 1/2$, it was proposed that the enhanced quantum fluctuations may completely destroy the long-range antiferromagnetic order (Anderson, 1973; Fazekas and Anderson, 1974). However, the spin-wave calculations suggested that the 120° state is stable for $S = 1/2$, albeit with a significantly reduced ordered moment (Jolicoeur and Le Guillou, 1989;

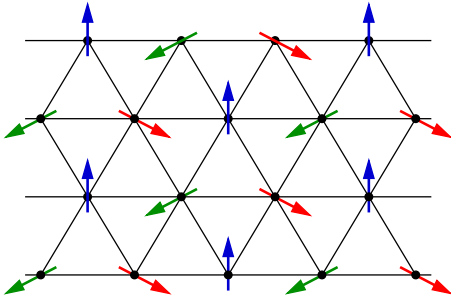


FIG. 12 (color online). The ordered 120° spin structure of the triangular-lattice Heisenberg antiferromagnet.

Miyake, 1992). The exact diagonalization of small clusters (Bernu *et al.*, 1994) together with the more recent QMC (Capriotti, Trumper, and Sorella, 1999), series-expansion (Zheng *et al.*, 2006b), and density-matrix renormalization group studies (White and Chernyshev, 2007) confirmed the stability of the 120° spin structure for the spin-1/2 case and yielded $\langle S \rangle \approx 0.20$ for the ordered moment.

The series-expansion results for the excitation spectrum of the spin-1/2 triangular-lattice antiferromagnet (Zheng *et al.*, 2006a) deviate substantially from the harmonic spin-wave theory with the overall band narrowing by $\sim 50\%$ and additional rotonlike minima. These effects were shown to result from strong magnon-magnon interactions by Starykh, Chubukov, and Abanov (2006) and Zheng *et al.* (2006b), who demonstrated that the first-order $1/S$ renormalization gives a spectrum in qualitative agreement with the series-expansion data. The importance of decays in the magnon spectrum of the triangular-lattice antiferromagnet was pointed out by Chernyshev and Zhitomirsky (2006).

We now proceed with a brief description of the spin-wave results for the dynamics of the triangular-lattice antiferromagnet, referring interested readers to Chernyshev and Zhitomirsky (2009a) for a detailed review. We consider the Heisenberg Hamiltonian (38) with the exchange interaction between the nearest-neighbor sites $J(\mathbf{r}) \equiv J\delta_{|\mathbf{r}|,1}$. In this case, the Fourier transform of the exchange matrix is $J_{\mathbf{q}} = 6J\gamma_{\mathbf{q}}$ with $\gamma_{\mathbf{q}} = \frac{1}{3}[\cos q_x + 2\cos(q_x/2)\cos(\sqrt{3}q_y/2)]$. The ordering wave vector of the 120° spin structure $\mathbf{Q} = (4\pi/3, 0)$ is commensurate with the reciprocal lattice and is located at the K point in the corner of the Brillouin zone; see Fig. 13.

The magnon dispersion in the harmonic approximation is

$$\varepsilon_{\mathbf{k}} = 3JS\sqrt{(1 - \gamma_{\mathbf{k}})(1 + 2\gamma_{\mathbf{k}})}. \quad (42)$$

In full agreement with the general picture outlined above, the excitation spectrum has three Goldstone modes at $\mathbf{k} = \mathbf{0}, \pm\mathbf{Q}$ with distinct spin-wave velocities c_0 and c_Q . In the harmonic approximation their ratio is $c_0/c_Q = \sqrt{2}$, with the leading $1/S$ renormalization reducing it to $c_0/c_Q \approx 1.156$ in the $S = 1/2$ case (Chubukov, Sachdev, and Senthil, 1994). Another notable feature of the dispersion in Eq. (42) is the varying convexity of the acoustic branch in the vicinity of the \mathbf{Q} points

$$\varepsilon_{\mathbf{Q}+\mathbf{k}} \approx c_Q k(1 - \alpha_\varphi k), \quad \alpha_\varphi \sim \cos 3\varphi, \quad (43)$$

which changes its sign depending on the direction of \mathbf{k} .

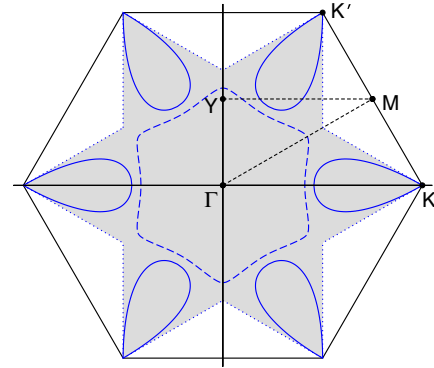


FIG. 13 (color online). Brillouin zone of the triangular lattice. The magnon decay region is shown as a shaded area. Solid and dashed lines indicate saddle-point van Hove singularities of the two-magnon continuum.

Using the harmonic expression for $\varepsilon_{\mathbf{k}}$ we obtain the magnon decay region of the triangular-lattice antiferromagnet as given by the shaded hexagram in Fig. 13. The decay threshold boundary is determined solely by the emission of an acoustic magnon with $\mathbf{q} \rightarrow \pm\mathbf{Q}$; see Eq. (17), shown in Fig. 13 by dotted lines. As anticipated above, the decay region includes an extended neighborhood of the Γ point. Interestingly, the decay region also extends all the way to the K, K' points ($\equiv \pm\mathbf{Q}$). This is a consequence of varying convexity of the corresponding acoustic branch (43) together with the commensurability of the ordering wave vector $3\mathbf{Q} = \mathbf{G}$. As a result, the kinematic conditions are satisfied for a decay from the steeper side of the energy cone with $\mathbf{k} \rightarrow \mathbf{Q}$ into two magnons with $\mathbf{q}, \mathbf{q}' \rightarrow -\mathbf{Q}$. Thus, magnons near K or K' points are unstable only in a certain range of angles, in agreement with Fig. 13.

In clear contrast with the field-induced decays (see Fig. 5), the decay region of the triangular-lattice antiferromagnet is not extended by the three-magnon decays. This implies that the cascade multimagnon decays do not have a tendency to spread over the Brillouin zone and that the decay threshold boundary remains sharp. The boundary can change due to renormalization of the harmonic dispersion (42), but the corresponding shifts appear to be not very significant (Chernyshev and Zhitomirsky, 2009a).

Last, the solid and dashed lines in Fig. 13 show the threshold boundaries for the emission of two equivalent and inequivalent magnons, respectively; see Sec. III.A. Both sets of contours lie completely within the decay region and thus correspond to the saddle points of the two-magnon continuum, which result in the logarithmic peaks in the magnon decay rate $\Gamma_{\mathbf{k}}$; see Sec. III.C.

The $1/S$ renormalization of the magnon spectrum of the triangular-lattice antiferromagnet is calculated in the same way as in the case of the square-lattice antiferromagnet, discussed in Sec. IV. The minor technical simplification is in the absence of the angle renormalization in the present case due to the high symmetry of the 120° state. Aside from this detail, the renormalized “on-shell” spectrum is given by Eq. (35) with the self-energies $\Sigma_a(\mathbf{k}, \varepsilon_{\mathbf{k}})$ and $\Sigma_b(\mathbf{k}, \varepsilon_{\mathbf{k}})$ [see Figs. 1(a) and 1(b)], and the Hartree-Fock correction from the quartic terms (30). All relevant expressions can be

found in Chernyshev and Zhitomirsky (2009a); see also Starykh, Chubukov, and Abanov (2006) for a somewhat different procedure of deriving the $1/S$ renormalization.

The magnon energy and the decay rate obtained in the $1/S$ approximation (35) are shown by dashed lines in Fig. 14 along the representative \mathbf{k} directions. In addition to the singularities, similar to the square-lattice case in Fig. 9, there is a significant reduction of the magnon bandwidth. This substantial downward energy renormalization is due to strong repulsion of one- and two-magnon states that are coupled by the cubic anharmonicities. One can expect such interactions to produce similarly strong downward shifts of the excitation energies in the other spiral antiferromagnets. For example, in the anisotropic XY limit of the $S = 1/2$ triangular-lattice antiferromagnet, reduction of the bandwidth due to magnon interactions is even stronger and exceeds 50% of the harmonic value (Chernyshev and Zhitomirsky, 2009a), a magnitude unheard of in the collinear antiferromagnets.

Finally, the magnon damping, the hallmark of magnon decays in spiral antiferromagnets, is substantial throughout much of the decay region of Fig. 13. As noted, the channel that determines the decay threshold boundary in the present case is the emission of the acoustic magnon. Because of that, the threshold behavior of the decay rate near the boundary in Fig. 14 is not singular, $\Gamma_{\mathbf{k}} \sim (k - k_b)^2$ (Chernyshev and Zhitomirsky, 2006), in contrast with the square-lattice case (see Fig. 9), where the threshold singularities are due to minima in the two-magnon density of states.

There is another important difference in the dynamics of two-particle decays in these two cases. Magnons emitted in an elementary decay process in the square-lattice antiferromagnet are also unstable. Allowing for a finite lifetime of the decay products using self-consistent dressing of Fig. 1(a) gave us divergence-free magnon damping in Sec. IV. For the triangular-lattice antiferromagnet this approach may not work as the emitted magnons are often stable. In particular, this is true for the vicinity of the logarithmic singularities indicated by solid lines in Fig. 13: the saddle-point momenta

of the two-magnon continuum, which are responsible for the singular behavior, can be shown to fall outside the decay region. Hence, at the saddle points, the logarithmic divergence of the one-loop diagrams will persist even for the renormalized spectrum and the singularities seem to remain essential. Thus, the construction of a renormalized theory seems to require a summation of an infinite series of diagrams that contain leading-order divergences, as in the Pitaevskii treatment of the spectrum termination problem (Pitaevskii 1959). Such a procedure is technically problematic as it goes beyond the standard $1/S$ spin-wave expansion and allows only for qualitative results (Chernyshev and Zhitomirsky, 2009a).

This seemingly hopeless situation is resolved if we note that the logarithmic singularity occurs for a magnon inside the decay region, which means that there is always a “background” of the nonsingular decays in $\Gamma_{\mathbf{k}}$. In that case, one has to allow for a finite lifetime of the *initial* magnon while magnons created during the decay process may remain stable. Technically, the corresponding procedure amounts to solving the “off-shell” Dyson equation for complex $\varepsilon = \bar{\varepsilon}_{\mathbf{k}} - i\Gamma_{\mathbf{k}}$, preserving causality by substituting $\varepsilon \rightarrow \varepsilon^*$ in the argument of the self-energy (Chernyshev and Zhitomirsky, 2009a). Then the Dyson equation is reduced to the system

$$\bar{\varepsilon}_{\mathbf{k}} = \varepsilon_{\mathbf{k}} + \text{Re}[\Sigma(\mathbf{k}, \varepsilon^*)], \quad \Gamma_{\mathbf{k}} = -\text{Im}[\Sigma(\mathbf{k}, \varepsilon^*)]. \quad (44)$$

The off-shell approach avoids complications related to higher-order multiloop diagrams and naturally regularizes the decay singularities in $\Gamma_{\mathbf{k}}$ and $\bar{\varepsilon}_{\mathbf{k}}$. Results obtained by numerically solving Eq. (44) are shown in Fig. 14 by solid lines. The decay rates remain significant even in the absence of logarithmic peaks reaching $\Gamma_{\mathbf{k}}/\bar{\varepsilon}_{\mathbf{k}} \sim 0.15$.

VI. DAMPING OF LOW-ENERGY MAGNONS

The long-wavelength limit is where one usually hopes to find universal behavior of the dynamical properties. It is also the regime where decay rates can be calculated perturbatively because of the smallness of interaction among low-energy excitations and due to reduction of the phase-space volume available for decay processes. In this section we discuss a few general scenarios for decays of the long-wavelength excitations with the goal of identifying universal dependencies of $\Gamma_{\mathbf{k}}$ on \mathbf{k} and complement it with particular examples from the triangular- and square-lattice antiferromagnets considered above.

As discussed in Sec. III.B, there are several typical situations for the overlap of the single-particle acoustic branch with the two-particle continuum that allows for energy conservation to be fulfilled in the decay process. Here we do not repeat this classification and assume that such conditions are always satisfied. Generally, the decay rate is given by

$$\Gamma_{\mathbf{k}} \sim \sum_{\mathbf{q}} |V_{\mathbf{k},\mathbf{q}}|^2 \delta(\varepsilon_{\mathbf{k}} - \varepsilon_{\mathbf{q}} - \varepsilon_{\mathbf{k}-\mathbf{q}}), \quad (45)$$

where $V_{\mathbf{k},\mathbf{q}}$ is the decay vertex. Because of energy conservation, the upper limit for the momentum of created quasiparticles should be of the order of k . Then for the linear spectrum $\varepsilon_{\mathbf{k}} \sim k$, a naive power counting suggests

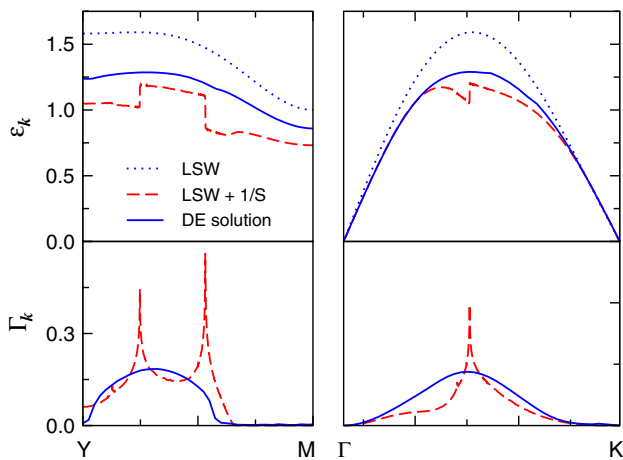


FIG. 14 (color online). Magnon energy and decay rate in units of J for the spin- $\frac{1}{2}$ triangular-lattice antiferromagnet. Dotted and dashed lines are the harmonic and the $1/S$ renormalized results, respectively. Solid lines are solutions of the Dyson equation (44) in the complex plane.

$$\Gamma_{\mathbf{k}} \sim k^{D-1} |V_{\mathbf{k}}|^2, \quad (46)$$

where k^D comes from the D -dimensional phase space, $1/k$ is due to the reduction of that space to the decay surface from energy conservation, and $V_{\mathbf{k}}$ is the typical amplitude of the cubic vertex on the decay surface. We assume that the cubic vertex at small momenta follows the standard ‘‘hydrodynamic’’ form (Lifshitz and Pitaevskii, 1980): $V_{\mathbf{k},\mathbf{q}} \propto \sqrt{kq q'}$, where $q' = |\mathbf{k} - \mathbf{q}|$, and that in a typical decay process all the momenta are of the same order $q, q' \sim k$. This makes $|V_{\mathbf{k}}|^2 \propto k^3$ and yields a seemingly universal power law for the decay rate of an arbitrary acoustic mode:

$$\Gamma_{\mathbf{k}} \sim k^{D+2}. \quad (47)$$

For $D = 3$, $\Gamma_{\mathbf{k}} \sim k^5$, which matches the well-known result for the decay of a phonon with a convex dispersion curve (Beliaev, 1958), but, as we see shortly, only coincidentally.

In reality, the situation is more delicate and possible power-law exponents for $\Gamma_{\mathbf{k}}$ vary depending on physical details. In the case of a single weakly nonlinear acoustic branch, relevant to phonons in ^4He , $\varepsilon_{\mathbf{k}} = ck + \alpha k^3$, decays are allowed only for the positive curvature $\alpha > 0$; see Sec. III.B. A long-wavelength phonon decays into a pair of quasiparticles with their momenta directed in a narrow solid angle along the direction of the initial momentum. The apex angle of the decay cone scales as $\theta \sim k$ such that the phase space is k^{2D-1} instead of the naive k^D . Then the restriction from energy conservation gives $1/k\theta^2 \sim 1/k^3$ instead of $1/k$ as considered previously. Altogether, for the case of the cubic upward curvature of the spectrum, the answer is universal [see also Kreisel *et al.* (2008)]:

$$\Gamma_{\mathbf{k}} \sim k^{2D-1}, \quad (48)$$

which indeed yields $\Gamma_{\mathbf{k}} \sim k^5$ in 3D (Beliaev, 1958; Lifshitz and Pitaevskii, 1980), but the answer for 2D is $\Gamma_{\mathbf{k}} \sim k^3$, different from Eq. (47). The 2D result applies to the square-lattice antiferromagnet in the strong field considered in Sec. IV.

If several acoustic modes with different velocities are present, the fast quasiparticle can always decay into two slow excitations (see Sec. III.B). This situation is simpler than in the previous case since the nonlinearity of the spectra plays no role. The phase-space factor becomes k^{D-1} now, in agreement with the naive consideration above. Physical realizations of this scenario include decays of the longitudinal phonon into two transverse ones in solids (Kosevich, 2005) as well as the decay of the $\mathbf{k} \rightarrow \mathbf{0}$ into two $\mathbf{k} \rightarrow \pm \mathbf{Q}$ magnons in the triangular-lattice Heisenberg antiferromagnet considered in Sec. V, a case also pertinent to other spiral antiferromagnets. Interaction between phonons in crystals obeys the conventional asymptotic behavior $V_{\mathbf{k},\mathbf{q}} \propto \sqrt{kq q'}$ and, consequently, $|V_{\mathbf{k}}|^2 \propto k^3$. Therefore, our initial naive power-counting result in Eq. (47) is, actually, valid for them. However, in the case of the triangular-lattice antiferromagnet, the result is yet different from that in Eq. (47) because the three-magnon vertex is anomalous and scales as $V_{\mathbf{k},\mathbf{Q}+\mathbf{q}} \propto (q' - q)\sqrt{k/q q'}$ for small k (Chernyshev and Zhitomirsky, 2009a). For a typical decay process the initial and final momenta are of the same order $q, q' \sim k$, giving $|V_{\mathbf{k},\mathbf{Q}+\mathbf{q}}|^2 \sim k$

instead of k^3 . Altogether, for noncollinear Heisenberg antiferromagnets in D dimensions this yields

$$\Gamma_{\mathbf{k}} \sim k^D. \quad (49)$$

Direct analytic calculation for long-wavelength magnons in the triangular antiferromagnet gives a decay rate with the correct exponent $\Gamma_{\mathbf{k}} \approx 0.79k^2$.

The decay vertex for the $\mathbf{k} \rightarrow \mathbf{Q}$ magnon has the conventional scaling $V_{\mathbf{Q}+\mathbf{k},-\mathbf{Q}+\mathbf{q}} \propto \sqrt{kq q'}$, so the decay probability is $|V_{\mathbf{k}}|^2 \sim k^3$. However, due to a constraint on the angle between \mathbf{k} and \mathbf{q} , the decay surface in \mathbf{q} space is a cigar-shaped ellipse with length $\sim k$ and width $\sim k^{3/2}$. That causes the restricted phase volume of decays to scale as $k^{(3D-5)/2}$ and leads to a nontrivial \mathbf{k} dependence of the decay rate:

$$\Gamma_{\mathbf{k}} \sim k^{(3D+1)/2}. \quad (50)$$

Numerically, in the triangular antiferromagnet $\Gamma_{\mathbf{k}} \approx 1.2Jk^{7/2}$ along the $K\Gamma$ line, in agreement with Eq. (50). Away from this direction, damping exhibits an anomalous angular dependence $\Gamma_{\mathbf{k}} \sim k^{7/2}/(\cos 3\varphi)^{3/2}$. It diverges upon approaching the decay threshold boundaries at $\varphi = \pm\pi/6$ in Fig. 13 and thus requires a self-consistent regularization.

Another case of the singular behavior of the decay rate in the long-wavelength limit occurs in the consideration of the square-lattice antiferromagnet in high fields; see Sec. IV. Here we outline an approach to regularizing such divergences (Mourigal, Zhitomirsky, and Chernyshev, 2010). Using the asymptotic form of the magnon dispersion in Eq. (18), the decay vertex $V_3^{(1)}(\mathbf{q}; \mathbf{k}) \propto \sqrt{kq q'}$, and the Born expression for the decay rate in Eq. (7) we obtain

$$\Gamma_{\mathbf{k}} = \frac{3J}{16\pi} \tan^2 \theta \sqrt{\frac{c}{6\alpha}} k^3, \quad (51)$$

in agreement with Eq. (48) with expressions for c and α provided in Eq. (32). An important observation is that the nonlinearity of the spectrum α vanishes at the decay threshold field $H \rightarrow H^*$, and, as a result, the coefficient in front of k^3 in Eq. (51) diverges. Such nonanalytic behavior is nothing but the long-wavelength version of the decay threshold singularities discussed in Sec. III.C. The self-consistent regularization (37) should remain applicable in this limit. In order to obtain the renormalized \mathbf{k} dependence of the damping, we substitute the general power-law ansatz for the decay rate $\Gamma_{\mathbf{k}} = \beta k^n$, and assume that the damping is much larger than the vanishing nonlinearity but still much smaller than the magnon energy $\alpha k^3 \ll \beta k^n \ll ck$. In this case, the apex angle of the decay cone scales as $\varphi^2 \sim k^{n-1}$ with $q \sim k$, which makes the decay vertex $V_3^{(1)}(\mathbf{q}; \mathbf{k}) \propto k^{n-3/2}$ instead of $k^{3/2}$. The power counting on both sides of Eq. (37) yields a unique solution $n = 3$. Therefore, the Born power law $\Gamma_{\mathbf{k}} = \beta k^3$ is not changed by the self-consistent procedure. The damping coefficient β no longer diverges near the decay threshold field because α drops out from the self-consistent equation for $\Gamma_{\mathbf{k}}$. Instead, β exhibits a steplike behavior in $H - H^*$, which is in accord with the 2D character of the van Hove singularity at the border of the two-particle continuum.

Another interesting asymptotic regime concerns the close vicinity of the saturation field with an almost parabolic

magnon dispersion. As $H \rightarrow H_s$, the velocity of the acoustic mode decreases and the condition of weak nonlinearity applies to a progressively narrower range of momenta $k \ll 4\sqrt{1 - H/H_s}$, reducing the range of validity of the asymptotic expression (51). Outside that \mathbf{k} domain one can use the parabolic form for magnon dispersion, $\varepsilon_{\mathbf{k}} \approx JSk^2$, to derive another useful asymptotic expression for the decay rate. In this regime the decay vertex is a constant $V_3^{(1)}(\mathbf{q}; \mathbf{k}) \propto \sqrt{1 - H/H_s}$, and the angle between the emitted and initial magnons can be large, removing restrictions from the decay phase space. Combining the power-counting arguments following Eq. (46) and performing analytical integration in Eq. (7) we obtain the universal momentum-independent expression

$$\Gamma_{\mathbf{k}} \approx 16 \left(1 - \frac{H}{H_s}\right), \quad (52)$$

which is valid for $4\sqrt{1 - H/H_s} \ll k \ll 1$.

VII. MAGNON DECAY IN QUANTUM SPIN LIQUIDS

Magnetic materials with quantum-disordered or spin-liquid-like ground states have attracted significant attention in the past two decades. The original idea goes back to Anderson (1973), who suggested the resonating-valence-bond singlet state as a candidate for a quantum-disordered ground state of the spin- $\frac{1}{2}$ triangular antiferromagnet. Since then, various types of spin-liquid ground states have been discussed and classified; see Dagotto and Rice (1996), Balents (2010), and Lhuillier and Misguich (2011). On the experimental side, well-known examples include the spin-Peierls compound CuGeO_3 (Hase, Terasaki, and Uchinokura, 1993), the dimer systems $\text{Cs}_3\text{Cr}_2\text{Br}_9$ (Leuenberger *et al.*, 1983) and TlCuCl_3 (Takatsu, Shiramura, and Tanaka, 1997), inter-spin antiferromagnetic chains (Regnault *et al.*, 1994), and many others. A common property of all these materials is the gap in the excitation spectrum, which separates a spin-singlet ground state from the triplet of magnetic excitations with $S = 1$. For that reason they are also referred to as quantum spin-gap magnets. The spin-spin correlations remain short ranged down to zero temperature with the correlation length inversely proportional to the gap $\xi \sim 1/\Delta$. Because of the threefold degeneracy, magnons in quantum spin-gap materials are often called triplons.

The spin-dimer magnets offer a particularly wide variety of quantum-disordered states regarding the energy scale of the spin gap and different effective dimensionalities. They became model systems for studying quantum phase transitions (Ruëgg *et al.*, 2008; Sachdev, 2008) and the field-induced Bose-Einstein condensation of magnons (Giamarchi and Tsvetlik, 1999; Nikuni *et al.*, 2000). For an overview of this subfield of quantum magnetism, see Grenier and Ziman (2007) and Giamarchi, Rugg, and Tchernyshyov (2008). Here we focus on the role of spontaneous magnon decays in the dynamics of quantum spin-gap magnets. Thereby, we exclude gapless 1D spin-liquid states with fractionalized spinon excitations as well as more exotic forms of spin liquids in higher dimensions that have yet to find a definitive experimental realization (Balents, 2010).

The theoretical attention paid to magnon decays is motivated by the inelastic neutron experiments in two organic quantum spin-gap materials piperazinium hexachlorodicyprate (PHCC) (Stone *et al.*, 2006) and $(\text{CH}_3)_2\text{CHNH}_3\text{CuCl}_3$ called IPA- CuCl_3 (Masuda *et al.*, 2006; Zheludev *et al.*, 2007) in which sharp transformation of triplet excitations upon crossing into the two-magnon continuum was observed. In PHCC, the magnon lifetime is seen rapidly decreasing once inside the continuum, whereas in IPA- CuCl_3 not even a trace of the single-particle peak is detected beyond the crossing. Such an end point was dubbed the termination point of the magnon branch by analogy with a similar effect in the superfluid ^4He (Lifshitz and Pitaevskii, 1980). The origin of this drastic effect was linked to the nonanalytic behavior of the magnon self-energy due to two-particle decays by Zhitomirsky (2006). The predicted behavior was confirmed by numerical simulations (Zheng, Hamer, and Singh, 2006; Fischer, Duffe, and Uhrig, 2010) and by an analytical model calculation (Bibikov, 2007). In this section we give an overview of theoretical results on two-magnon decays in quantum-gap antiferromagnets. We discuss a microscopic approach to spin-dimer magnets based on the bosonic representation of spins in terms of bond operators in Sec. VII.A. This is followed by an analysis of the termination point in the magnon dispersion curve; see Sec. VII.B. Discussion of the related problem of the decay of longitudinal magnons in weakly ordered antiferromagnets is included in Sec. VII.C.

A. Bond-operator formalism

One of the most studied models of quantum spin-dimer systems is the spin- $\frac{1}{2}$ ladder shown in Fig. 15(a). Its Hamiltonian is

$$\hat{\mathcal{H}} = J_{\perp} \sum_i \mathbf{S}_{1i} \cdot \mathbf{S}_{2i} + J \sum_{i,n=1,2} \mathbf{S}_{ni} \cdot \mathbf{S}_{ni+1}, \quad (53)$$

where J_{\perp} is an antiferromagnetic exchange along rungs and J is a coupling along the legs of the ladder. Such a model spin Hamiltonian is realized in a few magnetic compounds; see, for example, Notbohm *et al.* (2007) and Schmidiger *et al.* (2011). For $J_{\perp} \gtrsim J$, the ground state can be approximated by a product of singlet dimers occupying the rungs of the ladder. In this limit, properties of the spin ladder can be calculated

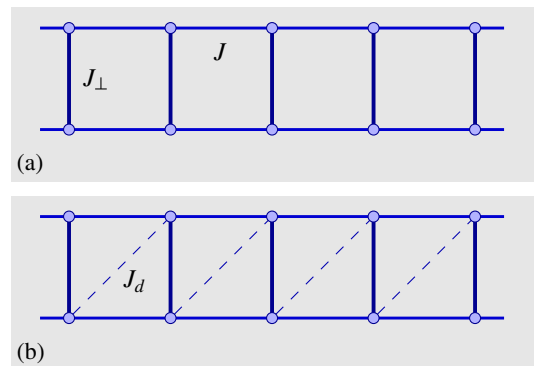


FIG. 15 (color online). Geometry of exchange bonds for (a) symmetric spin ladder and (b) asymmetric ladder with extra diagonal coupling.

using the bond-operator representation of spins proposed independently in several works (Harris, 1973; Chubukov, 1989; Sachdev and Bhatt, 1990).

Two spins $S = 1/2$ on the same rung can form one singlet $|s\rangle$ and three triplet states:

$$\begin{aligned} |s\rangle &= \frac{1}{\sqrt{2}}(|\uparrow\downarrow\rangle - |\downarrow\uparrow\rangle), & |t_+\rangle &= |\uparrow\uparrow\rangle, \\ |t_0\rangle &= \frac{1}{\sqrt{2}}(|\uparrow\downarrow\rangle + |\downarrow\uparrow\rangle), & |t_-\rangle &= |\downarrow\downarrow\rangle. \end{aligned} \quad (54)$$

In zero field it is more convenient to use the vector basis $|t_x\rangle = (|t_-\rangle - |t_+\rangle)/\sqrt{2}$, $|t_y\rangle = i(|t_-\rangle + |t_+\rangle)/\sqrt{2}$, and $|t_z\rangle = |t_0\rangle$; see Sachdev and Bhatt (1990). The representation of the original spin operators in the dimer basis is

$$S_{1,2}^\alpha = \pm \frac{1}{2}(s^\dagger t_\alpha + t_\alpha^\dagger s) - \frac{i}{2}\epsilon^{\alpha\beta\gamma} t_\beta^\dagger t_\gamma, \quad (55)$$

where we introduced singlet s^\dagger and triplet t_α^\dagger operators that create four physical states out of a fictitious vacuum $|0\rangle$. Bosonic commutation relations for s and t_α together with the constraint $s^\dagger s + t_\alpha^\dagger t_\alpha = 1$ ensure the standard SU(2) algebra for spins.

In the bond-operator representation (55), the spin Hamiltonian (53) takes the form $\hat{\mathcal{H}} = \hat{\mathcal{H}}_0 + \hat{\mathcal{H}}_2 + \hat{\mathcal{H}}_4$, where $\hat{\mathcal{H}}_0$ and $\hat{\mathcal{H}}_2$ are quadratic in t_α :

$$\begin{aligned} \hat{\mathcal{H}}_0 &= J_\perp \sum_i \left(-\frac{3}{4} s_i^\dagger s_i + \frac{1}{4} t_{\alpha i}^\dagger t_{\alpha i} \right), \\ \hat{\mathcal{H}}_2 &= \frac{J}{2} \sum_i (s_i^\dagger s_{i+1} t_{\alpha i+1}^\dagger t_{\alpha i} + s_i^\dagger s_{i+1}^\dagger t_{\alpha i+1} t_{\alpha i} + \text{H.c.}), \end{aligned} \quad (56)$$

whereas $\hat{\mathcal{H}}_4$ includes four-triplon terms. Next one needs to enforce the local constraint on the total number of singlets and triplets on each dimer. This can be achieved using various approximate schemes. One of them consists of condensing singlets s_i , $s_i^\dagger \rightarrow \langle s \rangle$, and fixing the boson density with the help of the chemical potential (Sachdev and Bhatt, 1990). Alternatively, the constraint is resolved in Holstein-Primakoff-like fashion, $s = s^\dagger = \sqrt{1 - t_\alpha^\dagger t_\alpha}$, and the square roots are expanded in powers of the triplon density (Chubukov, 1989). Although the final form of the effective Hamiltonian is somewhat different in the two approaches, the lowest-order magnon-magnon interaction contains only four-particle terms.

Suppose now that the crystal space group allows additional asymmetric diagonal coupling J_d between rungs of the ladder [see Fig. 15(b)]:

$$\hat{\mathcal{H}}_d = J_d \sum_i \mathbf{S}_{1i} \cdot \mathbf{S}_{2i+1}. \quad (57)$$

The bond-operator representation for $\hat{\mathcal{H}}_d$ yields a three-magnon interaction term

$$\hat{\mathcal{H}}_3 = \frac{J_d}{2} \langle s \rangle \sum_{k_i} \epsilon^{\alpha\beta\gamma} (\sin k_1 t_{k_1\alpha}^\dagger t_{k_2\beta}^\dagger t_{k_3\gamma} + \text{H.c.}), \quad (58)$$

which has the structure anticipated in Sec. II.D.

The difference in the magnon interaction between the two models [see Figs. 15(a) and 15(b)] has a symmetry origin. Three-magnon interactions are prohibited in a symmetric spin ladder because singlet states are antisymmetric under permutation of two spins while triplet states have even parity. However, if the reflection symmetry between the ladder legs is broken, coupling between one- and two-triplet sectors (58) is also allowed. Three-magnon interactions exist in many spin-dimer systems including the bond-alternating spin chain and various 2D and 3D arrays of dimers (Sachdev and Bhatt, 1990; Matsumoto *et al.*, 2004). Cubic terms have also been discussed for the Haldane-chain antiferromagnets (Zaliznyak, Lee, and Petrov, 2001; Kolezhuk and Sachdev, 2006). Finally, the geometry of exchange bonds in the spin-dimer magnet IPA-CuCl₃, which will be discussed in the next section, has precisely the structure shown in Fig. 15(b) (Masuda *et al.*, 2006; Fischer, Duffe, and Uhrig, 2011).

B. Termination point of the magnon branch

We now investigate the effects of three-magnon interactions for the generic energy spectrum of a quantum spin-gap magnet illustrated in Fig. 16. An important feature of the magnon dispersion is a minimum at a finite momentum due to antiferromagnetic correlations in the system. For simplicity, we consider only the most common case of a single minimum at a commensurate wave vector \mathbf{Q} . The overlap between the single-magnon branch and two-particle continuum occurs if the magnon bandwidth $W = \mathcal{O}(J)$ exceeds the gap $\Delta = \mathcal{O}(J_\perp)$; see Fig. 16. Then, naturally, the decay region is the range of momenta centered around $\mathbf{k} = \mathbf{0}$ and magnons that are created in a decay process are farther down the dispersion curve toward \mathbf{Q} and $-\mathbf{Q}$.

Following the kinematic analysis of Sec. III.A, in the absence of gapless Goldstone modes, the only two channels that may define the boundary of the decay region are the decays into magnons with equal momenta or equal velocities [cases (i) and (iv), respectively]. Considering the typical situation of a modest overlap with the continuum, i.e., when the magnon energy $\epsilon_c \gtrsim 2\Delta$, one can show that the prevailing channel is the former channel of equal momenta $\epsilon_{\mathbf{k}_c} = 2\epsilon_{(\mathbf{k}_c+\mathbf{G})/2}$, where \mathbf{G} is a reciprocal lattice vector.

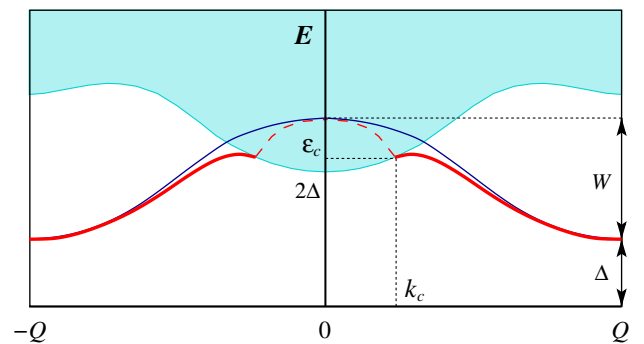


FIG. 16 (color online). Structure of the energy spectrum of a quantum spin-gap magnet. The thin solid line is the bare triplon energy $\epsilon_{\mathbf{k}}$, the full solid line is the renormalized dispersion $\bar{\epsilon}_{\mathbf{k}}$, and the shaded region is the two-particle continuum. The decay threshold is marked by k_c and ϵ_c .

The threshold boundary for the field-induced decays in square-lattice antiferromagnet (see Sec. IV), is of the same type, yet the kinematics is quite different here as the emitted magnons are outside the decay region and no cascadelike smearing of the boundary is possible. Thus, we encounter a kinematic situation distinct from the cases treated in Secs. IV and V, which requires detailed consideration of the spectrum near the decay boundary. As shown next, the presence of nonanalytic self-energy leads to dramatic qualitative changes of the magnon spectrum near the threshold.

According to the preceding discussion, the three-magnon interaction has the form

$$\hat{V}_3 = \frac{1}{2} \sum_{\mathbf{k}, \mathbf{q}} V_3(\mathbf{q}, \mathbf{k} - \mathbf{q}; \mathbf{k}) \epsilon^{\alpha\beta\gamma} (t_{\mathbf{q}\alpha}^\dagger t_{\mathbf{k}-\mathbf{q}\beta}^\dagger t_{\mathbf{k}\gamma} + \text{H.c.}). \quad (59)$$

Although due to conservation of the total spin the magnon with polarization γ can decay only into magnons with different polarizations, as enforced by the antisymmetric tensor $\epsilon^{\alpha\beta\gamma}$, this has no implications for the decays as long as the three branches remain degenerate. More important is the antisymmetric structure of the magnon vertex under the permutation of polarizations α and β and, consequently, under the interchange of momenta of the decay products $V_3(\mathbf{q}, \mathbf{q}'; \mathbf{k}) = -V_3(\mathbf{q}', \mathbf{q}; \mathbf{k})$. Since at the decay boundary the emitted magnons have equal momenta, the three-magnon vertex (59) vanishes at the threshold $V_3(\mathbf{q}^*, \mathbf{q}^*; \mathbf{k}_c) = 0$. Then the main difference from the analysis of the decay singularities in Sec. III.C is the effective increase of dimensionality due to further expansion of the decay vertex in $\tilde{\mathbf{q}} = \mathbf{q} - \mathbf{q}^*$ needed in the vicinity of the boundary:

$$\Sigma(\mathbf{k}, \omega) \simeq -g_3^2 \int_0^\Lambda \frac{\tilde{q}^{D+1} d\tilde{q}}{A\tilde{q}^2 + \mathbf{v}_2 \cdot \Delta\mathbf{k} - \Delta\omega - i0}, \quad (60)$$

where D is the dimension, $\Delta\omega = \omega - \varepsilon_c$, $\Delta\mathbf{k} = \mathbf{k} - \mathbf{k}_c$, \mathbf{v}_2 is the velocity of emitted magnons, $A = \mathcal{O}(J)$ is a constant, and $g_3 = \mathcal{O}(J_d)$ is an effective coupling constant. Because of the vanishing vertex, the self-energy (60) is not singular at the decay boundary $\Delta\omega$, $|\Delta\mathbf{k}| \rightarrow 0$ even in $D = 1$, but it is still nonanalytic. The higher-order corrections can be shown to leave unchanged the functional form of the nonanalyticity obtained in the one-loop approximation (60). Next we absorb the regular part of $\Sigma(\mathbf{k}, \omega)$ into the magnon energy $\varepsilon_{\mathbf{k}}$, while the renormalized spectrum will be obtained from the Dyson equation with the nonanalytic part $\tilde{\Sigma}(\mathbf{k}, \omega)$. We focus on the 1D case, mentioning a few results for the higher-dimensional systems in the end.

We begin with the region $k > k_c$ where spontaneous magnon decays are forbidden; see Fig. 16. In this case, integration in Eq. (60) yields the following nonanalytic self-energy:

$$\tilde{\Sigma}(k, \omega) = \lambda \sqrt{v_2 \Delta k - \Delta\omega}, \quad \Delta\omega < v_2 \Delta k, \quad (61)$$

with $\lambda = \pi g_3^2 / 2A^{3/2} = \mathcal{O}(J_d^2/J^{3/2})$. Close to the decay boundary the nonanalytic $\tilde{\Sigma}(k, \omega)$ dominates the regular part of $G^{-1}(k, \omega) \sim \Delta k, \Delta\omega$ and completely determines the behavior of the quasiparticle pole. Solving the Dyson equation with Eq. (61) yields the renormalized spectrum sketched in Fig. 16 (Zhitomirsky, 2006). Far away from the decay boundary the renormalized magnon energy $\tilde{\varepsilon}_k$ follows bare dispersion ε_k with the negative velocity $v_1 = d\varepsilon_k/dk < 0$.

On the other hand, for $k \rightarrow k_c$ the renormalized slope must change its sign to $d\tilde{\varepsilon}_k/dk = v_2 > 0$ as the minimum of the two-particle continuum at k_c is formed by magnons from the positive slope of ε_k . This change of the magnon velocity takes place in the crossover region $\Delta k \sim \lambda^2/(v_2 - v_1) = \mathcal{O}(J_d^2/J^2)$, and the overall shape of ε_k resembles the avoided crossing between the magnon branch $\tilde{\varepsilon}_k$ and the continuum boundary. However, due to the nonanalytic nature of the self-energy, the behavior of the spectrum is markedly different from the avoided crossing: the quasiparticle weight Z_k changes drastically in the crossover regime and vanishes at the intersection of the magnon branch with the two-magnon continuum. Such a suppression of the quasiparticle peak is a hallmark of the termination point in the energy spectrum, very similar to that in ^4He (Pitaevskii, 1959). In a different context, similar distortion of the excitation curve ε_k in the vicinity of the continuum boundary was also observed by Coldea *et al.* (2010).

For $k < k_c$, inside the continuum where spontaneous decays are allowed, the nonanalytic self-energy (60) is now purely imaginary:

$$\tilde{\Sigma}(k, \omega) = -i\lambda \sqrt{|v_2 \Delta k - \Delta\omega|}, \quad \Delta\omega > v_2 \Delta k. \quad (62)$$

Within the on-shell approximation, $\omega = \varepsilon_k$, this leads to the following magnon decay rate:

$$\Gamma_k \simeq \lambda \sqrt{(v_2 - v_1)|k - k_c|}. \quad (63)$$

The same result was obtained by Kolezhuk and Sachdev (2006). A more rigorous off-shell solution of the Dyson equation in the complex plane changes the perturbative result of Eq. (63) in the Δk vicinity [$\sim \mathcal{O}(J_d^2/J^2)$] of the decay boundary to $\Gamma_k \propto |k - k_c|^{2/3}$. However, more importantly, the quasiparticle weight remains suppressed in this region, in the same way as on the other side of the termination point. The quasiparticle peak may reappear farther away from the decay boundary depending on the strength of the three-magnon interaction.

We also note the common misconception regarding the absence of a pole beyond the termination point inside the two-particle continuum (Stone *et al.*, 2006). According to our analysis, such a pole is always present on either side of the termination point, but its quasiparticle residue is vanishingly small in the vicinity of that point.

The effect of spontaneous decays in the energy spectra of gapped spin liquids was studied numerically for the bond-alternating spin- $\frac{1}{2}$ chain by Zheng, Hamer, and Singh (2006b) and for the asymmetric ladder by Fischer, Duffe, and Uhrig (2010). For both models, the single-particle branch merges with the lower edge of the continuum, gradually losing its spectral weight. Fischer, Duffe, and Uhrig (2010) also found some indications of a reemerging quasiparticle peak inside the continuum for small values of the three-magnon coupling J_d .

A remarkable illustration of the theory is provided by the energy spectra measured in the spin-ladder compound IPA-CuCl₃ (Masuda *et al.*, 2006). This material consists of 2D arrays of weakly coupled asymmetric $S = 1/2$ Heisenberg ladders [see Fig. 15(b)], with the coupling constants $J_\perp = 2.9$ meV, $J = 1.2$ meV, $J_d = -2.3$ meV, and a

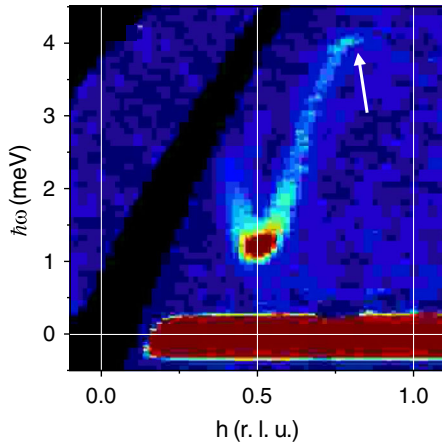


FIG. 17 (color online). Time-of-flight inelastic neutron-scattering data measured in IPA-CuCl₃ at $T = 1.5$ K (Masuda *et al.*, 2006). The arrow indicates the termination point of the magnon branch. From Andrey Zheludev.

small interladder exchange $J_{2D} \approx -0.3$ meV (Fischer, Duffe, and Uhrig, 2011). The resolution-limited peaks corresponding to the magnon band with a minimum at $Q = 0.5$ (units of $2\pi/a$) and the energy gap $\Delta = 1.2$ meV are observed in IPA-CuCl₃; see Fig. 17. However, the magnon branch abruptly disappears at $k_c \approx 0.8$. Using their data for $\varepsilon_{\mathbf{k}}$, Masuda *et al.* (2006) determined that k_c indeed corresponds to the intersection point of $\varepsilon_{\mathbf{k}}$ with the continuum. Thus, the single-magnon branch in IPA-CuCl₃ terminates at the boundary of the two-magnon continuum, as in the superfluid ⁴He, where the quasiparticle branch terminates at the threshold of two-roton decays (Pitaevskii, 1959; Glyde *et al.*, 1998).

A gradual broadening of the quasiparticle peak by two-magnon decays without its complete disappearance was observed in the 2D dimer organic material PHCC (Stone *et al.*, 2006) and in the quasi-1D antiferromagnet CsNiCl₃ (Zaliznyak, Lee, and Petrov, 2001). The difference from IPA-CuCl₃ discussed above is mainly due to the higher dimensionality of these two materials. In the case of PHCC, the experimental data are reasonably well described by Fermi's golden-rule formula

$$\Gamma_{\mathbf{k}}^{(D)} \simeq \lambda |\mathbf{k} - \mathbf{k}_c|^{D/2}, \quad (64)$$

with $D = 2$ (Kolezhuk and Sachdev, 2006). Beyond the on-shell approximation, the triplon self-energy (60) in $D > 1$ gives much weaker nonanalyticity. For example, in 2D, $\tilde{\Sigma}(\mathbf{k}, \omega) \sim \Delta \omega \ln(\Lambda/\Delta \omega)$, and the suppression of the quasiparticle peak in PHCC should occur only in an exponentially small region near the crossing point, justifying the validity of the perturbative result (64).

Thus far, we discussed spontaneous magnon decays in quantum spin-gap systems under the “standard” condition of the cubic vertex vanishing at the decay threshold boundary. The decay-related singularities may be substantially enhanced, however, if the vertex is finite. This takes place, for example, when the threshold channel corresponds to decays into magnons with different momenta. Another mechanism is spin anisotropy, which violates spin conservation and removes the odd parity of the cubic vertex (59) with respect

to spin indices and momenta, making the decay vertex finite at the continuum boundary and also lifting degeneracy of the triplon bands. This mechanism might be relevant to the spin-1 alternating chain antiferromagnet Ni(C₉H₂₄N₄)(NO₂)ClO₄ (called NTENP), whose unusual spin dynamics in an external magnetic field may signify spontaneous two-magnon decays (Hagiwara *et al.*, 2005; Regnault *et al.*, 2006). Finite magnetic fields also produce intriguing changes in the dynamical properties of IPA-CuCl₃ (Garlea *et al.*, 2007; Zheludev *et al.*, 2007). Theoretical explanation of these experimental findings remains an open problem.

Finally we note that the occurrence of the terminationlike behavior in the spectra of quantum spin-gap magnets is by no means unique. It can also take place in a variety of spin-anisotropic antiferromagnets (Chernyshev and Zhitomirsky, 2009a), in which the anisotropy gap stabilizes the decay products and makes the corresponding threshold singularities essential.

C. Decay of longitudinal magnons

Our final example of spontaneous magnon decays concerns weakly ordered collinear antiferromagnets, which occupy an intermediate place between quantum-disordered and well-ordered semiclassical magnets. Apart from the conventional spin waves, excitation spectrum of the weakly ordered spin system may display a longitudinal mode that corresponds to fluctuations of the magnitude of the order parameter (Affleck, 1989). The presence of this mode can be easily understood by considering a transition from the spin-liquid phase into an ordered state under an external pressure P (Matsumoto *et al.*, 2004). In the quantum-disordered state, up to the critical pressure P_c where the gap closes, three magnon modes are degenerate. Above the quantum transition, $P > P_c$, two of these modes transform into the Goldstone modes of the ordered magnetic structure, while the remaining third excitation acquires a finite gap. At this point one may ask how the above scenario could at all agree with the conventional spin-wave picture, which accounts only for the two magnon modes. The apparent contradiction is resolved if we notice that the longitudinal mode is always unstable with respect to decay into a pair of transverse spin waves and thus has an intrinsic linewidth (Affleck and Wellman, 1992). Farther inside the parameter domain of the ordered phase, the longitudinal excitation transforms into two-magnon resonance and eventually disappears.

The pressure-induced quantum critical point is realized, for instance, in the spin-dimer antiferromagnet TiCuCl₃ (Oosawa *et al.*, 2003). The low critical pressure $P_c \approx 1$ kbar enables the use of inelastic neutron measurements to explore the phases on both sides of the critical point. The existence of the gapped longitudinal mode in the antiferromagnetic phase of TiCuCl₃ was demonstrated by Ruëgg *et al.* (2008), who concluded that such a mode is “critically well defined” because of its large broadening. Recently, the lifetime of longitudinal excitations in TiCuCl₃ was calculated by Kulik and Sushkov (2011). In the following, we describe basic aspects of spontaneous magnon decays in weakly ordered collinear antiferromagnets using the example of TiCuCl₃.

The harmonic theory of magnetic excitations in both disordered and ordered phases of TiCuCl_3 was developed by [Matsumoto *et al.* \(2004\)](#) who used the bond-operator formalism. At the critical pressure $P = P_c$ the gap of the triplon branch closes at the commensurate ordering wave vector \mathbf{Q} . No spontaneous decays of the low-energy magnons exist up to this point. At $P > P_c$ one member of the degenerate triplet condenses, $t_{iz} \rightarrow \langle t_z \rangle e^{i\mathbf{Q}\cdot\mathbf{r}_i}$, and the collinear magnetic structure develops along the corresponding direction. The degeneracy of the triplon bands is removed in the ordered phase. Transverse excitations $t_{x,y}$ stay degenerate with each other and remain gapless with the energy $\varepsilon_{\mathbf{Q}+\mathbf{k}}^\perp \approx ck$, whereas the fluctuating part of the condensed magnon $\tilde{t}_z = t_z - \langle t_z \rangle$ represents the longitudinal mode with the energy $\varepsilon_{\mathbf{k}}^z$ and the gap $\Delta_L = \varepsilon_{\mathbf{Q}}^z \propto \sqrt{P - P_c}$.

Although the cubic vertex (59) may be absent in the disordered state at $P < P_c$, the triplet condensation in the ordered phase always produces a three-particle interaction involving longitudinal fluctuations; see Eq. (4): $t_{\alpha\mathbf{k}_4}^\dagger t_{\alpha\mathbf{k}_3}^\dagger t_{\beta\mathbf{k}_2}^\dagger t_{\beta\mathbf{k}_1} \rightarrow \langle t_z \rangle \tilde{t}_{z\mathbf{k}_3}^\dagger t_{\beta\mathbf{k}_2}^\dagger t_{\beta\mathbf{k}_1}$. Thus, the symmetry ensures that the longitudinal magnon can decay into a pair of transverse magnons $\beta = x, y$. Both energy and momentum conservation are also trivially satisfied for the decay of the gapped mode in the vicinity of the ordering wave vector \mathbf{Q} . The asymptotic form of the decay vertex is $V_3(\mathbf{q}, \mathbf{q}'; \mathbf{k}) \approx \langle t_z \rangle / (\varepsilon_{\mathbf{k}}^z \varepsilon_{\mathbf{q}}^\perp \varepsilon_{\mathbf{q}'}^\perp)^{1/2}$ ([Kulik and Sushkov, 2011](#)). In the bond-operator formalism, the anomalous denominator in V_3 with $\varepsilon_{\mathbf{Q}+\mathbf{q}}^\perp \approx cq$ appears from the coefficients of the Bogolyubov transformation. The decay rate of the longitudinal magnon at $\mathbf{k} = \mathbf{Q}$ calculated from Eq. (7) is

$$\Gamma_{\mathbf{Q}} \approx \frac{\langle t_z \rangle^2}{\Delta_L} = \gamma \Delta_L, \quad (65)$$

where the final relation follows from the mean-field result for the expectation value of the condensate fraction $\langle t_z \rangle \propto \sqrt{P - P_c}$. The theoretical estimate of the damping coefficient $\gamma = 0.2$ is not far from the experimental value $\gamma \approx 0.15$ and can be further improved upon by taking into account spin anisotropy in TiCuCl_3 ([Kulik and Sushkov, 2011](#)). Thus, the decay rate of the longitudinal mode is only parametrically small compared to its energy and whether it remains well defined depends on microscopic parameters of the system.

VIII. SUMMARY AND OUTLOOK

We presented an overview of the phenomenon of spontaneous magnon decays in quantum antiferromagnets and discussed symmetry and kinematic conditions that are necessary for it. While no exhaustive list of magnets that favor quasi-particle decays can be given, the offered examples outline the principal classes of spin systems, in which the effect may occur. Generally, the noncollinear spin structures in the systems where the symmetry is broken spontaneously from the high-symmetry spin Hamiltonian belong to one of such classes. The gapped quantum spin liquids is yet another class and a proximity to a quantum critical point can be another common situation in which magnetic excitations may be intrinsically damped.

The hallmarks of the decay-induced anomalies in magnon spectra include substantial broadening of magnon peaks in a large part of the Brillouin zone, termination points, and non-Lorentzian features in the structure factor, as well as strong deviations of the spectrum from the harmonic theory, especially for $S = 1/2$ systems. With improvement in the resolution of neutron-scattering experiments expected in the near future, these effects should become readily observable. Besides their effect on the dynamical properties, magnon decays may also play a role in the critical behavior in the vicinity of quantum critical points ([Fritz *et al.*, 2011](#)).

We also highlighted the role of singularities, which are generally concomitant with decays and are related to the crossing of the single-particle branch with the surface of van Hove singularities in the two-particle continuum. Regularization of such singularities represents a theoretical challenge that is largely unfamiliar in the traditional spin-wave theory and requires the use of self-consistent schemes exemplified in this work. While most of the systems considered here are 1D or 2D, for which the effects of spontaneous magnon decays are amplified, the strong effects due to spontaneous decays are not restricted to low-dimensional systems, as shown in Sec. IV.

The direct experimental evidence of magnon decays in low-dimensional spin-dimer systems discussed in Sec. VII is unequivocal and progress is being made toward similar observations in the noncollinear and field-induced settings. For the latter case, several materials with sufficiently small interactions that allow magnetic fields to fit into the window accessible by neutron-scattering experiments have recently been synthesized and the first indication of field-induced magnon decays has been found in the spin- $\frac{5}{2}$ square-lattice antiferromagnet $\text{Ba}_2\text{MnGe}_2\text{O}_7$ ([Masuda *et al.*, 2010](#)). As noted in Sec. IV, the BEC magnets are also very promising for the observation of the field-induced decays in the vicinity of their lower quantum critical point, which is readily accessible in a number of them. The experimental search for spontaneous magnon decays in noncollinear magnets is also ongoing, with several $S = 1/2$ triangular-lattice antiferromagnets, such as Cs_2CuBr_4 ([Tsujii *et al.*, 2007](#)) and $\text{Ba}_3\text{CoSb}_2\text{O}_9$ ([Shirata *et al.*, 2012](#)), and also the large- S weakly anisotropic noncollinear antiferromagnets ([Ishii *et al.*, 2011](#); [Toth *et al.*, 2011](#)) being most promising.

Besides improvements in conventional neutron scattering, there has been a recent dramatic improvement in neutron-spin-echo spectroscopy technique; see [Pappas, Ehlers, and Mezei \(2006\)](#). The energy resolution of this method can reach the μeV range compared to the meV resolution for triple-axis spectroscopy. Successful measurements of magnon lifetimes by the neutron-spin-echo technique were reported by [Bayrakci *et al.* \(2006\)](#), [Náfrádi *et al.* \(2011\)](#), and [Chernyshev *et al.* \(2012\)](#) and more of such studies are forthcoming. This development may offer an opportunity to observe a variety of new physical effects including spontaneous magnon decays.

Finite magnon lifetimes can also be detected by experimental probes other than the neutron scattering. One such example is the decay-related smearing observed by electron spin resonance in the bond-alternating chain antiferromagnet NTENP ([Glazkov *et al.*, 2010](#)). Another promising experimental

technique is resonant inelastic x-ray scattering (Ament *et al.*, 2011), which is able to detect excitation broadening in large-exchange spin systems. The magnetic component of thermal conductivity should also be strongly influenced by spontaneous magnon decays (Kohama *et al.*, 2011).

ACKNOWLEDGMENTS

We thank our co-workers, W. Fuhrman, M. Mourigal, and V. Stephanovich, for their contributions to this work and O. Syljuåsen and A. Zheludev for providing figures for this article. We are grateful to I. Affleck, C. Batista, W. Brenig, A. Chubukov, R. Coldea, F. Essler, N. Hasselmann, G. Jackeli, E. Kats, P. Kopietz, B. Lake, A. Läuchli, A. Muratov, B. Normand, N. Perkins, L.-P. Regnault, H. Rønnow, Ch. Rüegg, O. Starykh, O. Sushkov, I. Zaliznyak, and A. Zheludev for insightful discussions. This work was supported by the DOE under Grant No. DE-FG02-04ER46174 (A. L. C.).

REFERENCES

- Affleck, I., 1989, *Phys. Rev. Lett.* **62**, 474.
 Affleck, I., 1991, *Phys. Rev. B* **43**, 3215.
 Affleck, I., and G.F. Wellman, 1992, *Phys. Rev. B* **46**, 8934.
 Akhizer, A. I., V.G. Bar'yakhtar, and S. V. Peletminskii, 1968, *Spin Waves* (North-Holland, Amsterdam).
 Ament, L. J. P., M. van Veenendaal, T. P. Devereaux, J. P. Hill, and J. van den Brink, 2011, *Rev. Mod. Phys.* **83**, 705.
 Anderson, P. W., 1952, *Phys. Rev.* **86**, 694.
 Anderson, P. W., 1973, *Mater. Res. Bull.* **8**, 153.
 Anderson, P. W., 1984, *Basic Notions of Condensed Matter Physics* (Benjamin-Cummings, Menlo Park).
 Andreev, A. F., and V. I. Marchenko, 1980, *Usp. Fiz. Nauk* **130**, 39 [*Sov. Phys. Usp.* **23**, 21 1980].
 Balents, L., 2010, *Nature (London)* **464**, 199.
 Batyev, E. G., and L. S. Braginskii, 1984, *Zh. Eksp. Teor. Fiz.* **87**, 1361 [*Sov. Phys. JETP* **60**, 781 1984] [<http://www.jetp.ac.ru/cgi-bin/e/index/e/60/4/p781?a=list>].
 Bayrakci, S. P., T. Keller, K. Habicht, and B. Keimer, 2006, *Science* **312**, 1926.
 Beaurepaire, E., 2006, Ed., *Magnetism: A Synchrotron Radiation Approach* (Springer, Berlin).
 Beliaev, S. T., 1958, *Zh. Eksp. Teor. Fiz.* **34**, 433 [*Sov. Phys. JETP* **7**, 299 1958].
 Bernu, B., P. Lecheminant, C. Lhuillier, and L. Pierre, 1994, *Phys. Rev. B* **50**, 10048.
 Bibikov, P. N., 2007, *Phys. Rev. B* **76**, 174431.
 Bloch, F., 1930, *Z. Phys.* **61**, 206.
 Borovik-Romanov, A. S., and S. K. Sinha, 1988, Eds., *Spin-Waves and Magnetic Excitations* (Elsevier, Amsterdam).
 Brockhouse, B. N., 1995, *Rev. Mod. Phys.* **67**, 735.
 Capriotti, L., A. E. Trumper, and S. Sorella, 1999, *Phys. Rev. Lett.* **82**, 3899.
 Chakravarty, S., B. I. Halperin, and D. R. Nelson, 1989, *Phys. Rev. B* **39**, 2344.
 Chernyshev, A. L., 2012, *Phys. Rev. B* **86**, 060401(R).
 Chernyshev, A. L., and M. E. Zhitomirsky, 2006, *Phys. Rev. Lett.* **97**, 207202.
 Chernyshev, A. L., and M. E. Zhitomirsky, 2009a, *Phys. Rev. B* **79**, 144416.
 Chernyshev, A. L., and M. E. Zhitomirsky, 2009b, *Phys. Rev. B* **79**, 174402.
 Chernyshev, A. L., M. E. Zhitomirsky, N. Martin, and L.-P. Regnault, 2012, *Phys. Rev. Lett.* **109**, 097201.
 Chubukov, A. V., 1984, *J. Phys. C* **17**, L991.
 Chubukov, A. V., 1989, *Pis'ma Zh. Eksp. Teor. Fiz.* **49**, 108 [*Sov. Phys. JETP Lett.* **49**, 129 1989] [http://www.jetpletters.ac.ru/ps/1113/article_16848.shtml].
 Chubukov, A. V., S. Sachdev, and T. Senthil, 1994, *J. Phys. Condens. Matter* **6**, 8891.
 Coldea, R., D. A. Tennant, A. M. Tsvetlik, and Z. Tylczynski, 2001, *Phys. Rev. Lett.* **86**, 1335.
 Coldea, R., D. A. Tennant, E. M. Wheeler, E. Wawrzynska, D. Prabhakaran, M. Telling, K. Habicht, P. Smeibid, and K. Kiefer, 2010, *Science* **327**, 177.
 Coomer, F. C., *et al.*, 2007, *Phys. Rev. B* **75**, 094424.
 Dagotto, E., and T. M. Rice, 1996, *Science* **271**, 618.
 Dalidovich, D., R. Sknepnek, A. J. Berlinsky, J. Zhang, and C. Kallin, 2006, *Phys. Rev. B* **73**, 184403.
 de Groot, H. J. M., and L. J. de Jongh, 1986, *Physica (Amsterdam)* **141B+C**, 1.
 de Jongh, L. J., and A. R. Miedema, 1974, *Adv. Phys.* **23**, 1.
 Dombre, T., and N. Read, 1989, *Phys. Rev. B* **39**, 6797.
 Dyson, F. J., 1956a, *Phys. Rev.* **102**, 1217.
 Dyson, F. J., 1956b, *Phys. Rev.* **102**, 1230.
 Fazekas, P., and P. W. Anderson, 1974, *Philos. Mag.* **30**, 423.
 Fischer, T., S. Duffe, and G. S. Uhrig, 2010, *New J. Phys.* **12**, 033048.
 Fischer, T., S. Duffe, and G. S. Uhrig, 2011, *Europhys. Lett.* **96**, 47001.
 Fritz, L., R. L. Doretto, S. Wessel, S. Wenzel, S. Burdin, and M. Vojta, 2011, *Phys. Rev. B* **83**, 174416.
 Fuhrman, W. T., M. Mourigal, M. E. Zhitomirsky, and A. L. Chernyshev, 2012, *Phys. Rev. B* **85**, 184405.
 Garlea, V. O., *et al.*, 2007, *Phys. Rev. Lett.* **98**, 167202.
 Giamarchi, T., C. Ruegg, and O. Tchernyshyov, 2008, *Nat. Phys.* **4**, 198.
 Giamarchi, T., and A. M. Tsvetlik, 1999, *Phys. Rev. B* **59**, 11398.
 Glazkov, V. N., A. I. Smirnov, A. Zheludev, and B. C. Sales, 2010, *Phys. Rev. B* **82**, 184406.
 Gluzman, S., 1993, *Z. Phys. B* **90**, 313.
 Glyde, H. R., M. R. Gibbs, W. G. Stirling, and M. A. Adams, 1998, *Europhys. Lett.* **43**, 422.
 Graf, E. H., V. J. Minkiewicz, H. B. Moller, and L. Passell, 1974, *Phys. Rev. A* **10**, 1748.
 Grenier, B., and T. Ziman, 2007, *C.R. Physique* **8**, 717.
 Gurevich, A. G., and G. A. Melkov, 1996, *Magnetization Oscillations and Waves* (CRC Press, Boca Raton).
 Hagiwara, M., *et al.*, 2005, *Phys. Rev. Lett.* **94**, 177202.
 Hamer, C. J., Zheng Weihong, and P. Arndt, 1992, *Phys. Rev. B* **46**, 6276.
 Harris, A. B., 1973, *Phys. Rev. B* **7**, 3166.
 Harris, A. B., D. Kumar, B. I. Halperin, and P. C. Hohenberg, 1971, *Phys. Rev. B* **3**, 961.
 Hase, M., I. Terasaki, and K. Uchinokura, 1993, *Phys. Rev. Lett.* **70**, 3651.
 Hoddeson, L., G. Baym, and M. Eckert, 1987, *Rev. Mod. Phys.* **59**, 287.
 Holstein, T., and H. Primakoff, 1940, *Phys. Rev.* **58**, 1098.
 Igarashi, J.-I., 1992, *Phys. Rev. B* **46**, 10763.
 Igarashi, J.-I., and T. Nagao, 2005, *Phys. Rev. B* **72**, 014403.
 Ishii, R., *et al.*, 2011, *Europhys. Lett.* **94**, 17001.
 Jaime, M., *et al.*, 2004, *Phys. Rev. Lett.* **93**, 087203.

- Jolicœur, Th., and J. C. Le Guillou, 1989, *Phys. Rev. B* **40**, 2727.
- Kats, E. I., and A. R. Muratov, 2005, *J. Phys. Condens. Matter* **17**, 6849.
- Kohama, Y., *et al.*, 2011, *Phys. Rev. Lett.* **106**, 037203.
- Kohno, M., O. A. Starykh, and L. Balents, 2007, *Nat. Phys.* **3**, 790.
- Kolezhuk, A., and S. Sachdev, 2006, *Phys. Rev. Lett.* **96**, 087203.
- Kosevich, A. M., 2005, *The Crystal Lattice: Phonons, Solitons, Dislocations, Superlattices* (Wiley Verlag, Weinheim).
- Kreisel, A., F. Sauli, N. Hasselmann, and P. Kopietz, 2008, *Phys. Rev. B* **78**, 035127.
- Kubo, R., 1952, *Phys. Rev.* **87**, 568.
- Kulik, Y., and O. P. Sushkov, 2011, *Phys. Rev. B* **84**, 134418.
- Lancaster, T., *et al.*, 2007, *Phys. Rev. B* **75**, 094421.
- Leuenberger, B., H. U. Güdel, R. Feile, and J. K. Kjems, 1983, *Phys. Rev. B* **28**, 5368(R).
- Lhuillier, C., and G. Misguich, 2011, in *Introduction to Frustrated Magnetism*, edited by C. Lacroix (Springer, Berlin).
- Lifshitz, E. M., and L. P. Pitaevskii, 1980, *Statistical Physics II* (Pergamon, Oxford).
- Lüscher, A., and A. M. Läuchli, 2009, *Phys. Rev. B* **79**, 195102.
- Mahan, G. D., 2000, *Many-Particle Physics* (Kluwer, New York).
- Majlis, N., 2007, *The Quantum Theory of Magnetism* (World Scientific, Singapore).
- Manousakis, E., 1991, *Rev. Mod. Phys.* **63**, 1.
- Masuda, T., S. Kitaoka, S. Takamizawa, N. Metoki, K. Kaneko, K. C. Rule, K. Kiefer, H. Manaka, and H. Nojiri, 2010, *Phys. Rev. B* **81**, 100402(R).
- Masuda, T., A. Zheludev, H. Manaka, L.-P. Regnault, J.-H. Chung, and Y. Qiu, 2006, *Phys. Rev. Lett.* **96**, 047210.
- Matan, K., D. Grohol, D. G. Nocera, T. Yildirim, A. B. Harris, S. H. Lee, S. E. Nagler, and Y. S. Lee, 2006, *Phys. Rev. Lett.* **96**, 247201.
- Matsubara, T., and H. Matsuda, 1956, *Prog. Theor. Phys.* **16**, 569.
- Matsumoto, M., B. Normand, T. M. Rice, and M. Sigrist, 2004, *Phys. Rev. B* **69**, 054423.
- Mattis, D. C., 1981, *The Theory of Magnetism* (Springer, Berlin).
- Mila, F., 1998, *Eur. Phys. J. B* **6**, 201.
- Miyake, S. J., 1992, *J. Phys. Soc. Jpn.* **61**, 983.
- Mourigal, M., M. E. Zhitomirsky, and A. L. Chernyshev, 2010, *Phys. Rev. B* **82**, 144402.
- Náfrádi, B., T. Keller, H. Manaka, A. Zheludev, and B. Keimer, 2011, *Phys. Rev. Lett.* **106**, 177202.
- Nikuni, T., M. Oshikawa, A. Oosawa, and H. Tanaka, 2000, *Phys. Rev. Lett.* **84**, 5868.
- Notbohm, S., *et al.*, 2007, *Phys. Rev. Lett.* **98**, 027403.
- Oguchi, T., 1960, *Phys. Rev.* **117**, 117.
- Ohyama, T., and H. Shiba, 1993, *J. Phys. Soc. Jpn.* **62**, 3277.
- Oosawa, A., M. Fujisawa, T. Osakabe, K. Kakurai, and H. Tanaka, 2003, *J. Phys. Soc. Jpn.* **72**, 1026.
- Osano, K., H. Shiba, and Y. Endoh, 1982, *Prog. Theor. Phys.* **67**, 995.
- Pappas, C., G. Ehlers, and F. Mezei, 2006, in *Neutron Scattering From Magnetic Materials*, edited by T. Chatterji (Elsevier, Amsterdam).
- Pethick, C. J., and H. Smith, 2008, *Bose-Einstein Condensation in Dilute Gases* (Cambridge University Press, Cambridge).
- Pitaevskii, L. P., 1959, *Zh. Eksp. Teor. Fiz.* **36**, 1168 [*Sov. Phys. JETP* **9**, 830 1959].
- Pomeranchuk, I., 1941, *J. Phys. (USSR)* **IV**, 357.
- Regnault, L.-P., I. Zaliznyak, J. P. Renard, and C. Vettier, 1994, *Phys. Rev. B* **50**, 9174.
- Regnault, L.-P., A. Zheludev, M. Hagiwara, and A. Stunault, 2006, *Phys. Rev. B* **73**, 174431.
- Rößler, U. K., A. N. Bogdanov, and C. Pfleiderer, 2006, *Nature (London)* **442**, 797.
- Ruëgg, Ch., B. Normand, M. Matsumoto, A. Furrer, D. F. McMorrow, K. W. Krämer, H.-U. Güdel, S. N. Gvasaliya, H. Mutka, and M. Boehm, 2008, *Phys. Rev. Lett.* **100**, 205701.
- Sachdev, S., 2008, *Nat. Phys.* **4**, 173.
- Sachdev, S., and R. N. Bhatt, 1990, *Phys. Rev. B* **41**, 9323.
- Sandvik, A. W., 1997, *Phys. Rev. B* **56**, 11678.
- Sandvik, A. W., and R. R. P. Singh, 2001, *Phys. Rev. Lett.* **86**, 528.
- Schmidiger, D., S. Mühlbauer, S. N. Gvasaliya, T. Yankova, and A. Zheludev, 2011, *Phys. Rev. B* **84**, 144421.
- Schulz, H. J., 1996, *Phys. Rev. Lett.* **77**, 2790.
- Shirata, Y., H. Tanaka, A. Matsuo, and K. Kindo, 2012, *Phys. Rev. Lett.* **108**, 057205.
- Slater, J. C., 1930, *Phys. Rev.* **35**, 509.
- Sluckin, T. J., and R. M. Bowley, 1974, *J. Phys. C* **7**, 1779.
- Starykh, O. A., A. V. Chubukov, and A. G. Abanov, 2006, *Phys. Rev. B* **74**, 180403(R).
- Stephanovich, V. A., and M. E. Zhitomirsky, 2011, *Europhys. Lett.* **95**, 17007.
- Stone, M. B., I. A. Zaliznyak, T. Hong, C. L. Broholm, and D. H. Reich, 2006, *Nature (London)* **440**, 187.
- Syljuåsen, O. F., 2008, *Phys. Rev. B* **78**, 180413(R).
- Syromyatnikov, A. V., 2009, *Phys. Rev. B* **79**, 054413.
- Syromyatnikov, A. V., 2010, *J. Phys. Condens. Matter* **22**, 216003.
- Takatsu, K., W. Shiramura, and H. Tanaka, 1997, *J. Phys. Soc. Jpn.* **66**, 1611.
- Toth, S., *et al.*, 2011, *Phys. Rev. B* **84**, 054452.
- Tsujii, H., C. R. Rotundu, T. Ono, H. Tanaka, B. Andraka, K. Ingersent, and Y. Takano, 2007, *Phys. Rev. B* **76**, 060406(R).
- Tsyrlin, N., T. Pardini, R. R. P. Singh, F. Xiao, P. Link, A. Schneidewind, A. Hiess, C. P. Landee, M. M. Turnbull, and M. Kenzelmann, 2009, *Phys. Rev. Lett.* **102**, 197201.
- Tsyrlin, N., F. Xiao, A. Schneidewind, P. Link, H. M. Rønnow, J. Gavilano, C. P. Landee, M. M. Turnbull, and M. Kenzelmann, 2010, *Phys. Rev. B* **81**, 134409.
- Van Kranendonk, J., and J. H. Van Vleck, 1958, *Rev. Mod. Phys.* **30**, 1.
- Veillette, M. Y., A. J. A. James, and F. H. L. Essler, 2005, *Phys. Rev. B* **72**, 134429.
- Villain, J., 1974, *J. Phys. (Paris)* **35**, 27.
- Walker, C. T., and G. A. Slack, 1970, *Am. J. Phys.* **38**, 1380.
- Weihong, Z., and C. J. Hamer, 1993, *Phys. Rev. B* **47**, 7961.
- White, R. M., 1983, *Quantum Theory of Magnetism* (Springer, Berlin).
- White, S. R., and A. L. Chernyshev, 2007, *Phys. Rev. Lett.* **99**, 127004.
- Woodward, F. M., A. S. Albrecht, C. M. Wynn, C. P. Landee, and M. M. Turnbull, 2002, *Phys. Rev. B* **65**, 144412.
- Xiao, F., *et al.*, 2009, *Phys. Rev. B* **79**, 134412.
- Zaliznyak, I. A., S.-H. Lee, and S. V. Petrov, 2001, *Phys. Rev. Lett.* **87**, 017202.
- Zheludev, A., *et al.*, 2007, *Phys. Rev. B* **76**, 054450.
- Zheng, W., J. O. Fjaerestad, R. R. P. Singh, R. H. McKenzie, and R. Coldea, 2006a, *Phys. Rev. Lett.* **96**, 057201.
- Zheng, W., J. O. Fjaerestad, R. R. P. Singh, R. H. McKenzie, and R. Coldea, 2006b, *Phys. Rev. B* **74**, 224420.
- Zheng, W., C. J. Hamer, and R. R. P. Singh, 2006, *Phys. Rev. B* **74**, 172407.

- Zheng, W., J. Oitmaa, and C.J. Hamer, 2005, *Phys. Rev. B* **71**, 184440.
- Zhitomirsky, M. E., 2006, *Phys. Rev. B* **73**, 100404(R).
- Zhitomirsky, M. E., and A. L. Chernyshev, 1999, *Phys. Rev. Lett.* **82**, 4536.
- Zhitomirsky, M. E., and T. Nikuni, 1998, *Phys. Rev. B* **57**, 5013.